Earth and Environmental Science Transactions of the Royal Society of Edinburgh, **111**, 173–192, 2020

Article

A review of the stem amniote *Eldeceeon rolfei* from the Viséan of East Kirkton, Scotland

Marcello RUTA[1]*, Jennifer A. CLACK[2] and Timothy R. SMITHSON[2]

[1] School of Life Sciences, Joseph Banks Laboratories, University of Lincoln, Green Lane, Lincoln LN6 7DL, UK.
[2] University Museum of Zoology, Downing Street, Cambridge CB2 3EJ, UK.
*Corresponding author. Email: mruta@lincoln.ac.uk

ABSTRACT: The late Viséan anthracosauroid *Eldeceeon rolfei* from the East Kirkton Limestone of Scotland is re-described. Information from two originally described and two newly identified specimens broadens our knowledge of this tetrapod. A detailed account of individual skull bones and a revision of key axial and appendicular features are provided, alongside the first complete reconstructions of the skull and lower jaw and a revised reconstruction of the postcranial skeleton. In comparison to *Silvanerpeton*, the only other anthracosauroid from East Kirkton, *Eldeceeon* is characterised by a proportionally wider semi-elliptical skull, comparatively smaller nostrils set farther apart, smaller and more rounded orbits, a shorter skull table with gently convex lateral margins, and a deeper suspensorium with a straight posterior margin and a small dorsal embayment. The remarkably large hind feet and elongate toes of *Eldeceeon* presumably represent an adaptation for attaining high locomotory speed through increased stride length and reduced stride frequency. This would necessitate great muscle force but few muscle contractions. At the beginning of a new stride cycle, repositioning the pes anteriorly and lifting the toes off the ground would require a strong and large muscle to pull the femur upward and rotate it inward and forward. It is hypothesised that such muscle might correspond to the *puboischiofemoralis internus 2*, which would extend along the posterior half of the vertebral column, consistent with the occurrence of long, curved ribs in the anterior half of the trunk. Using maximum parsimony and Bayesian inference, cladistic analyses of all major groups of stem amniotes retrieve a sister group relationship between *Eldeceeon* and *Silvanerpeton*, either as the most plesiomorphic stem amniote clade or as a clade immediately crownward of anthracosauroids.

KEY WORDS: anthracosauroids, early Carboniferous, phylogeny, postcranial skeleton, *Silvanerpeton*, skull, terrestrialisation.

Fossils from the late Viséan (upper part of the Middle Mississippian) volcanic lake deposits of East Kirkton near Bathgate (West Lothian, Scotland) first rose to prominence in the mid-1980s, when the late Stan Wood (Fraser *et al*. 2018) relocated an abandoned limestone quarry following meticulous inspection of the lithology of stone blocks employed by locals to build farm boundary walls (Clack 2017). Stan's painstaking efforts opened a new era in the study of Carboniferous faunas and floras, revealing the earliest and most complete assemblage of terrestrial biotas known to date (Rolfe *et al*. 1994; Clack 2012). Tetrapods are the best known and most celebrated of all taxonomic groups represented at East Kirkton. They are morphologically and taxonomically diverse, with seven named species known from fairly complete skeletons and additional, partially preserved specimens awaiting formal description (Clack 2012, 2017). The tetrapod grade-group known as the 'lepospondyls' (Carroll *et al*. 1998; discussion in Clack *et al*. 2019) is represented at East Kirkton by the aïstopod *Ophiderpeton kirktonense* Milner, 1994, the putative microsaur *Kirktonecta milnerae* Clack, 2011, and perhaps also *Westlothiana lizziae* Smithson & Rolfe, 1990, the latter taxon considered to be the earliest known amniote at the time of its discovery (Smithson 1989; Smithson *et al*. 1994), but subsequently re-interpreted as a stem amniote with possible basal 'lepospondyl' or microsaur affinities (Ruta *et al*. 2003; Ruta & Coates 2007; Clack & Milner 2015; Clack *et al*. 2016, 2019; Marjanović & Laurin 2019) or even as a stem tetrapod (Laurin & Reisz 1999). *Eucritta melanolimnetes* Clack, 1998 shares characters with groups as diverse as baphetids, temnospondyls, and anthracosaurs (Clack 2001); perhaps unsurprisingly, this combination of features has resulted in alternative phylogenetic placements for this taxon, either as a derived stem tetrapod or as a basal crown tetrapod shifting between alternate positions on either side of the lissamphibian–amniote dichotomy (Ruta *et al*. 2003; Ruta & Coates 2007; Clack & Milner 2015; Clack *et al*. 2016, 2019; Marjanović & Laurin 2019). Temnospondyls – the largest radiation of early tetrapods – are represented by *Balanerpeton woodi* Milner & Sequeira, 1994, the earliest known representative of this group, and currently regarded either as one of its most plesiomorphic members or as a more derived taxon (Ruta & Bolt 2006; Schoch 2013; Schoch & Milner 2014; Marjanović & Laurin 2019). Lastly, anthracosauroids (for a review of the use of this term in the early tetrapod literature, see Smithson 1985; Panchen & Smithson 1988; Laurin 2001; Ruta & Clack 2006) include *Silvanerpeton miripedes* Clack, 1994, which was redescribed by Ruta & Clack (2006), and *Eldeceeon rolfei* Smithson, 1994, which is the subject of this paper. *Silvanerpeton* emerged as the most basal stem amniote in Ruta & Clack's (2006) cladistic analysis (see also Clack & Finney

 doi:10.1017/S1755691020000079
https://doi.org/10.1017/S1755691020000079 Published online by Cambridge University Press

2005; Clack & Klembara 2009), but in a more derived position along the amniote stem in some subsequent studies (e.g., immediately crownward of anthracosauroids and close to gephyrostegids; Schoch *et al.* 2010; Clack *et al.* 2016, 2019; Witzmann & Schoch 2018; Arbez *et al.* 2019; Marjanović & Laurin 2019).

Smithson's (1994) description of *Eldeceeon* was based upon two specimens – the holotype and a second specimen. He was able to describe most of the postcranial material in considerable detail, but the skull was poorly preserved in both specimens. In particular, only the rearmost part of the holotype skull was known. Smithson (1994) highlighted a number of features, such as the presacral count and the limb proportions, in which *Eldeceeon* differs significantly from *Silvanerpeton*. These features were recently summarised by Clack & Milner (2015; see also diagnosis below). Since the original description, two more specimens of *Eldeceeon* have been identified. Together, all four specimens give a clearer picture of the skull and supply additional details of various postcranial elements. As a result, it is possible to provide a fuller new treatment of this tetrapod and to evaluate its phylogenetic affinities in a formal cladistic analysis. Alongside other East Kirkton 'reptiliomorphs' (*sensu* Säve-Söderbergh 1934; see Laurin 2001), including *Silvanerpeton* and *Westlothiana*, *Eldeceeon* is a key taxon for our understanding of morphological conditions near the evolutionary roots of the amniote total group (Pardo *et al.* 2017; Ford & Benson 2019; Klembara *et al.* 2020).

The aim of this paper is threefold: (1) we redescribe in detail *Eldeceeon*, emphasising characteristics of its cranial and postcranial anatomy for which new and/or additional information is available; (2) we compare *Eldeceeon* with a range of other 'reptiliomorphs', revising features of possible diagnostic values and drawing attention to those that differ in subtle ways from corresponding traits in other taxa (notably, *Silvanerpeton*); and (3) we build a phylogeny of (chiefly) Permian and Carboniferous stem amniotes in order to establish the position of *Eldeceeon* under alternative criteria for tree reconstruction.

1. Material and methods

1.1. Specimen preparation, photography, and illustrations

Specimen UMZC T.1350 was partly prepared by Lorie J. Barber (formerly at the Bristol Museum and Art Gallery). The specimen was consolidated with a thin layer of B-98 (polyvinyl butyral) solution in ethanol. Matrix was removed in places (e.g., pelves, partially preserved skull, appendicular skeleton, part of the axial skeleton) using pneumatic (Chicago Pneumatic®; Microjack® #2/4) and fine preparation tools (pin vices). Photography was undertaken by J. A. Clack using a Panasonic Lumix DMC-LZ5 followed by processing with Photoshop CC 2019. The stippled skull reconstruction of *Eldeceeon* was produced by M. Ruta. The labelled lateral view of the skull was supplied by J. A. Clack. The full skeletal reconstruction was provided by T. R. Smithson. Specimens were drawn by M. Ruta using a Wild M3 dissecting microscope equipped with a camera lucida and rendered using a combination of black ink and graphite.

1.2. Specimen measurements

Estimates of various measurement ratios relied upon a simple protocol designed to reduce measurement bias. High-resolution photographs were imported into the free software ImageJ2 (https://imagej.nih.gov/ij/). We applied the 'Straight Line' tool to measure linear distances of interest at high magnification (pixel resolution). This tool provides a direct reading of the length of a segment in arbitrary units, independent of image magnification and/or orientation. The measurements thus obtained were employed in ratio calculations. Each measurement was taken three times at intervals of 10 min, and the mean of the three recorded values was used.

1.3. Phylogenetic analysis

We built a cladistic matrix of 54 taxa and 291 osteological characters, representing an updated and expanded version of the matrix in Klembara *et al.* (2020), to which *Eldeceeon* was added (see Supplementary Material S1 and S2 available at https://doi.org/10.1017/S1755691020000079 for the list of characters and the data matrix). The matrix was subjected to tree searches with maximum parsimony in PAUP* 4.0a build 165 (https://paup.phylosolutions.com; Swofford 1998) and with Bayesian inference in MrBayes 3.2.6 (https://nbisweden.github.io/MrBayes/download.html; Ronquist & Huelsenbeck 2003).

Before running parsimony analyses, we inspected the matrix for possible occurrences of 'taxonomically equivalent' taxa (*sensu* Wilkinson 1996) using the R package *Claddis* (Lloyd 2016; see https://cran.r-project.org). All parsimony analyses (see section 4) employed identical tree search settings, as follows: (1) 'collapse branch' option enforced for branches possibly attaining a minimum length of zero; (2) heuristic search; (3) tree bisection-reconnection branch-swapping algorithm using 10,000 random stepwise taxon addition sequence replicates and keeping one tree in memory for each replicate; and (4) five consecutive branch-swapping rounds applied to all trees in memory following the 10,000 replicates and saving multiple trees. With maximum parsimony, we explored three schemes of character weighting, namely: (1) characters with equal unit weights; (2) characters reweighted by the maximum value (best fit) of their rescaled consistency indexes obtained from the equally weighted analysis; and (3) implied character weights (Goloboff 1993). For tree searches using implied weights, we compared the results obtained from a small selection of integer values of Goloboff's K constant of concavity ($K = 3, 6, 9, 12$; for discussions of K, see Goloboff *et al.* 2018). Given the maximum possible number of steps M and the actual observed number of steps O that a character exhibits on a tree, the implied weight W of that character is equivalent to $K / [K + M - O]$ for any given value of K. The implied weights procedure seeks to find the tree topology for which the sum of all W values across all characters is greatest. With equally weighted characters, we also calculated tree node support using bootstrapping (Felsenstein 1985) and jackknifing (Farris *et al.* 1996), in both cases using the fast stepwise addition option in PAUP* with 10,000 random character resampling replicates (in the case of jackknifing, 50% of all characters were resampled in each replicate).

The Bayesian analysis employed the standard data type option (morphological characters) with variable coding setting (accounting for uninformative characters) and a gamma-distributed rate model of state changes in effect. In total, we ran four chains with 10^7 generations, sampling every 1000 generations and discarding 25% of the obtained samples. At the end of the Bayesian search, we saved both branch lengths and clade credibility values, the latter providing measures of tree node support. We used Gelman & Rubin's (1992) Potential Scale Reduction Factor (PSRF) to test for satisfactory convergence.

2. Systematic palaeontology

Tetrapoda Jaekel, 1909 (*fide* Sues, 2019)
Amniota Haeckel, 1866 (reported *in errore* as Goodrich, 1916 by Ruta & Clack 2006)
(Stem group of Amniota herewith)
Family undesignated
Genus *Eldeceeon* Smithson, 1994
***Eldeceeon rolfei* Smithson, 1994**
(Figs 1–7)

https://doi.org/10.1017/S1755691020000079 Published online by Cambridge University Press

Holotype. National Museums Scotland (NMS) G.1986.39.1 (Fig. 1).

Referred material. NMS G.1990.7.1, part and counterpart (Figs 2, 3); University Museum of Zoology, Cambridge (UMZC) T.2013.3, part and counterpart (Figs 4, 5); UMZC T.1350 (Fig. 6).

Locality, age, and horizon. The type specimen was retrieved from a farm boundary wall (Smithson 1994). NMS G.1990.7.1 was collected from Unit 76 at the East Kirkton Quarry, near Bathgate, West Lothian, Scotland; Brigantian, Late Viséan, upper part of Middle Mississippian; East Kirkton Limestone, Bathgate Hills Volcanic Formation, Strathclyde Group (Rolfe *et al*. 1994). UMZC T.2013.3 and T.1350 were collected by Mr S. P. Wood, but no data were recorded by him. They might have been collected from one of the farm walls purchased by Mr Wood, or from one of the spoil heaps at the quarry.

Diagnosis. The diagnosis is after Clack & Milner (2015), modified from Smithson (1994), and with our additions/clarification in bold and italics. Comments on some characters are embedded in brackets. Where possible, we have tried to characterise features as either plesiomorphic for post-Devonian early tetrapods, certainly from among stem-amniote groups, or autapomorphic for *Eldeceeon*. We acknowledge, however, that a proper differential diagnosis remains difficult.

Uncertain polarity. Overall length at least 35 cm. Intercentra and pleurocentra similar in length, with large notochordal foramen (together, these features may be unique to *Eldeceeon*, but we note that the size of the notochordal foramen may be partly ontogenetic, and the similar lengths of intercentra and pleurocentra may well be autapomorphic).

Autapomorphies. Uniquely characterised by having *long, curved* ribs on only the first 14 to 16 of the 24 to 26 presacral vertebrae. Very short tabular horn. Little emargination at the back of the skull table *in the form of slight embayment immediately ventral to point where squamosal contacts skull table. Supratemporal much larger than intertemporal* (possibly unique among various stem-amniote groups, but noted in other early tetrapods, such as baphetids). Short neural spines anteriorly, which become progressively longer posteriorly.

Synapomorphies. Suspensorium short, *with nearly straight posterior margin* (various degrees of anteroposterior shortening of the suspensorium are observed in various stem-amniote groups – for instance, seymouriamorphs and diadectomorphs – although the shape and orientation of the free margin of the squamosal is variable).

Plesiomorphies. Narrow premaxillae and vomers (possibly generalised features for various stem-amniote groups). Broad pterygoids. Closed palate (this and the preceding feature are observed in several stem-amniote groups, such as seymouriamorphs, as well as in other early tetrapods including baphetids). Vertebrae gastrocentrous. Well-ossified appendicular skeleton. Interclavicle with very long parasternal process. Carpus unossified. Manus with phalangeal formula 2-3-4-5-4. Ilium with long post-iliac process. Large hind limbs. Eight ossified tarsals in each foot. Pedal phalangeal formula of 2-3-4-5-4. Extensive ventral squamation of long narrow scales.

3. Description

3.1. Skull roof

3.1.1. General features. As reconstructed (Fig. 7a–d), the skull of *Eldeceeon* resembles that of *Silvanerpeton* (Ruta & Clack 2006, fig. 8) but there are several differences between these taxa (see also Supplementary Material S3 and description of individual bones below). (1) The skull of *Eldeceeon* has a distinct semi-elliptical outline, unlike the parabolic skull of *Silvanerpeton*, and is proportionally slightly wider than the latter in relation to its length. (2) *Eldeceeon* has proportionally slightly smaller and more rounded orbits than *Silvanerpeton*, and comparatively smaller external nostrils situated farther apart than those of *Silvanerpeton*. (3) The skull table of *Eldeceeon* is comparatively more abbreviated than that of *Silvanerpeton* and with gently convex lateral margins; in contrast, these margins are nearly straight and obliquely orientated in *Silvanerpeton*. (4) The suspensorium of *Eldeceeon* is deeper in lateral aspect than that of *Silvanerpeton* and with a nearly straight posterior margin (gently concave in *Silvanerpeton*) that is slightly embayed immediately ventral to the point where the squamosal contacts the skull table. Compared to Smithson's (1994) reconstruction of the skull in lateral view, our reconstruction shows much larger orbits and external nostrils, a more abbreviated snout with a much steeper profile, and a shorter suspensorium characterised by a steeper and straighter posterior margin and a more pronounced dorsal embayment.

While acknowledging the difficulty of working from heavily disrupted material, we think the new skull reconstruction takes into account all available evidence. A possible contentious point is represented by the width of the skull at the level of the basipterygoid articulations. What little information is available on the palatines suggests that these bones were broad and, even allowing for a more oblique orientation of these bones, there appears to be no evidence that the palate was strongly vaulted. We do acknowledge, however, that the transverse flange of the pterygoid might have approached or contacted the medial surface of the jugal. This would confer a narrower projected surface area to the orbit in dorsal projection, but, even so, the orbit area would remain conspicuous, as suggested by the proportions of the circumorbital bones.

3.1.2. Dermal ornament. As in the case of *Silvanerpeton*, *Eldeceeon* shows no traces of lateral line canals (Figs 2c, 5c, d). The dermal ornament is well preserved on most skull roof bones, and is more variable and more accentuated than that of *Silvanerpeton*. The dominant pattern, such as is observed on the nasals, frontals, parietals, squamosals, and jugals (Fig. 7a–c), consists of small pits, slender ridges, shallow grooves, and low protuberances. Pits, ridges, and grooves mostly radiate out from the ossification centres of those bones. More peripherally, the ornament consists of fine striations, but sparse grooves and pits are also observed. Irregularly distributed foramina dot the external surface of the bones and are more densely packed on and around the ossification centres. On the squamosals, the ornament is particularly well developed (Fig. 2b, c). The ossification centre forms a slightly raised irregular area situated below the posterodorsal corner of the squamosal (in lateral aspect), from which strong ridges and grooves radiate out in a characteristic fan-like pattern. A similar, raised subtriangular area is visible on the main corpus of the jugal (Fig. 5b, d). The prefrontals and postfrontals exhibit an irregular ornament of fine, tightly appressed ridges and grooves distributed around the axis of greater anteroposterior curvature of those bones (Figs 2b, c, 5b, d). In striking contrast, the sculpture on the postorbital appears to vary in a mediolateral direction, with two distinct areas separated by a robust longitudinal ridge (Fig. 2b): the medial area carries fine longitudinal striations and shallow grooves, whereas the lateral area is occupied by deep pits and grooves. Although the squama of the lacrimal is heavily disrupted (Fig. 5b), preserved fragments show a coarse ornament of irregular, mostly longitudinal crests delimiting depressions. More posteriorly, along the suborbital ramus, the sculpture of the lacrimal changes into shallow grooves and low ridges, and this pattern continues smoothly posteriorly along the suborbital ramus and posteroventral surface of the jugal. A low relief, pustulose

https://doi.org/10.1017/S1755691020000079 Published online by Cambridge University Press

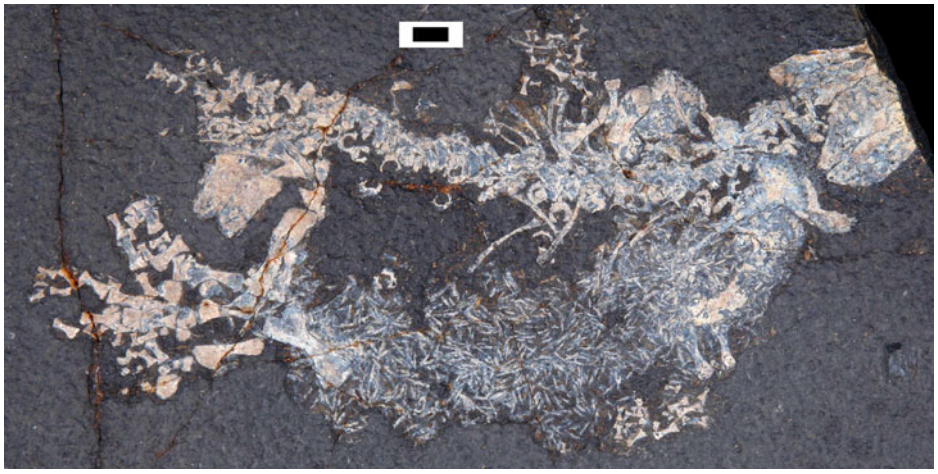

Figure 1 *Eldeceeon rolfei*. Photograph of holotype NMS G.1986.39.1. Scale bar = 20 mm.

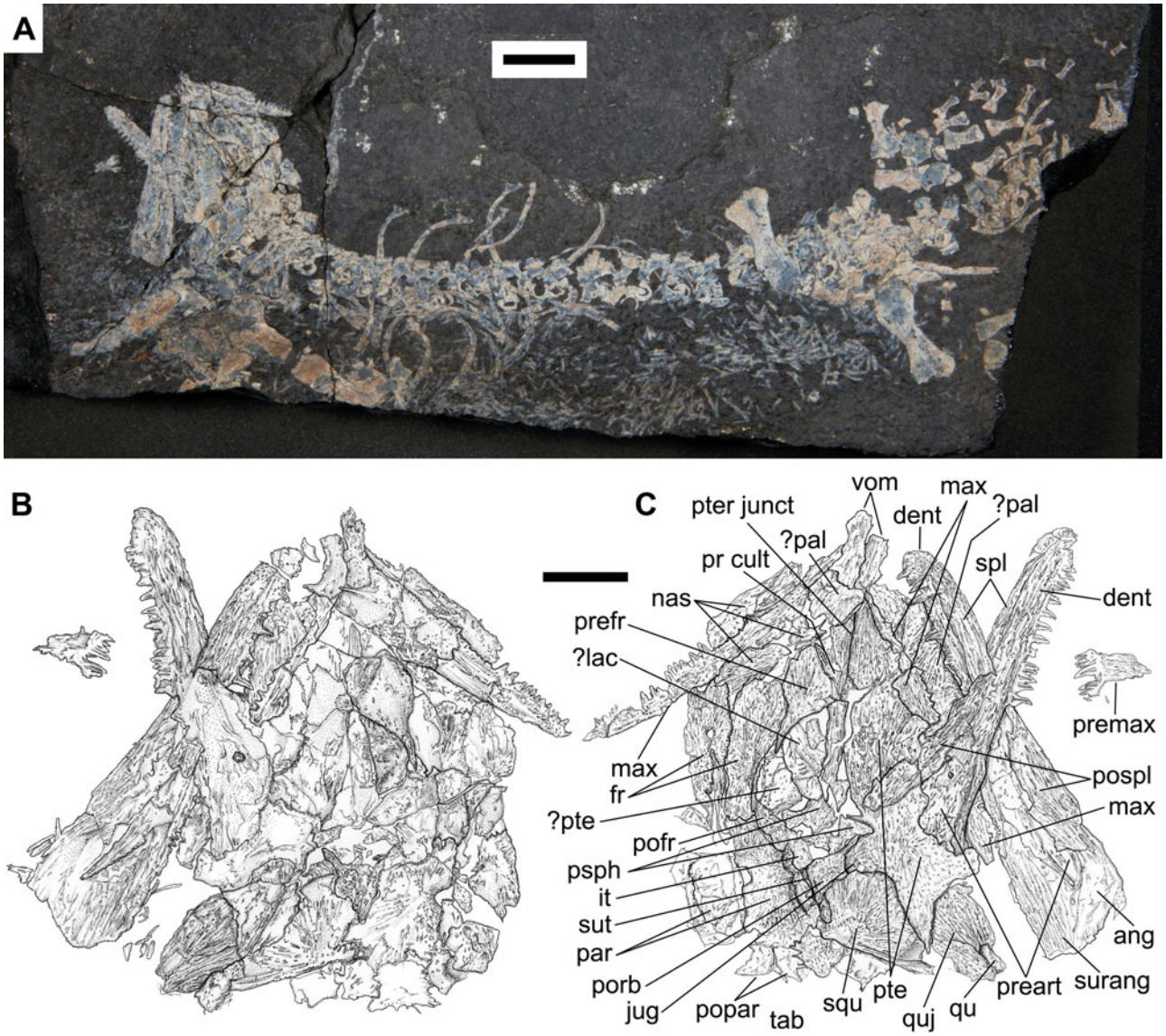

Figure 2 *Eldeceeon rolfei*. (A) Photograph of NMS G.1990.7.1a (part). (B) Interpretive drawing of NMS G.1990.7.1a (skull; part). (C) Interpretive drawing of NMS G.1990.7.1b (skull; counterpart). Abbreviations: ang = angular; dent = dentary; fr = frontal; it = intertemporal; jug = jugal; lac = lacrimal; max = maxilla; nas = nasal; pal = palatine; par = parietal; pofr = postfrontal; popar = postparietal; porb = postorbital; pospl = postsplenial; pr cult = cultriform process; preart = prearticular; prefr = prefrontal; premax = premaxilla; psph = basiparasphenoid; pte = pterygoid; pter junct = sutural junction between palatal rami of pterygoids; qu = quadrate; quj = quadratojugal; spl = splenial; squ = squamosal; surang = surangular; sut = supratemporal; tab = tabular; vom = vomer. Scale bars = 20 mm (A); 10 mm (B, C).

https://doi.org/10.1017/S1755691020000079 Published online by Cambridge University Press

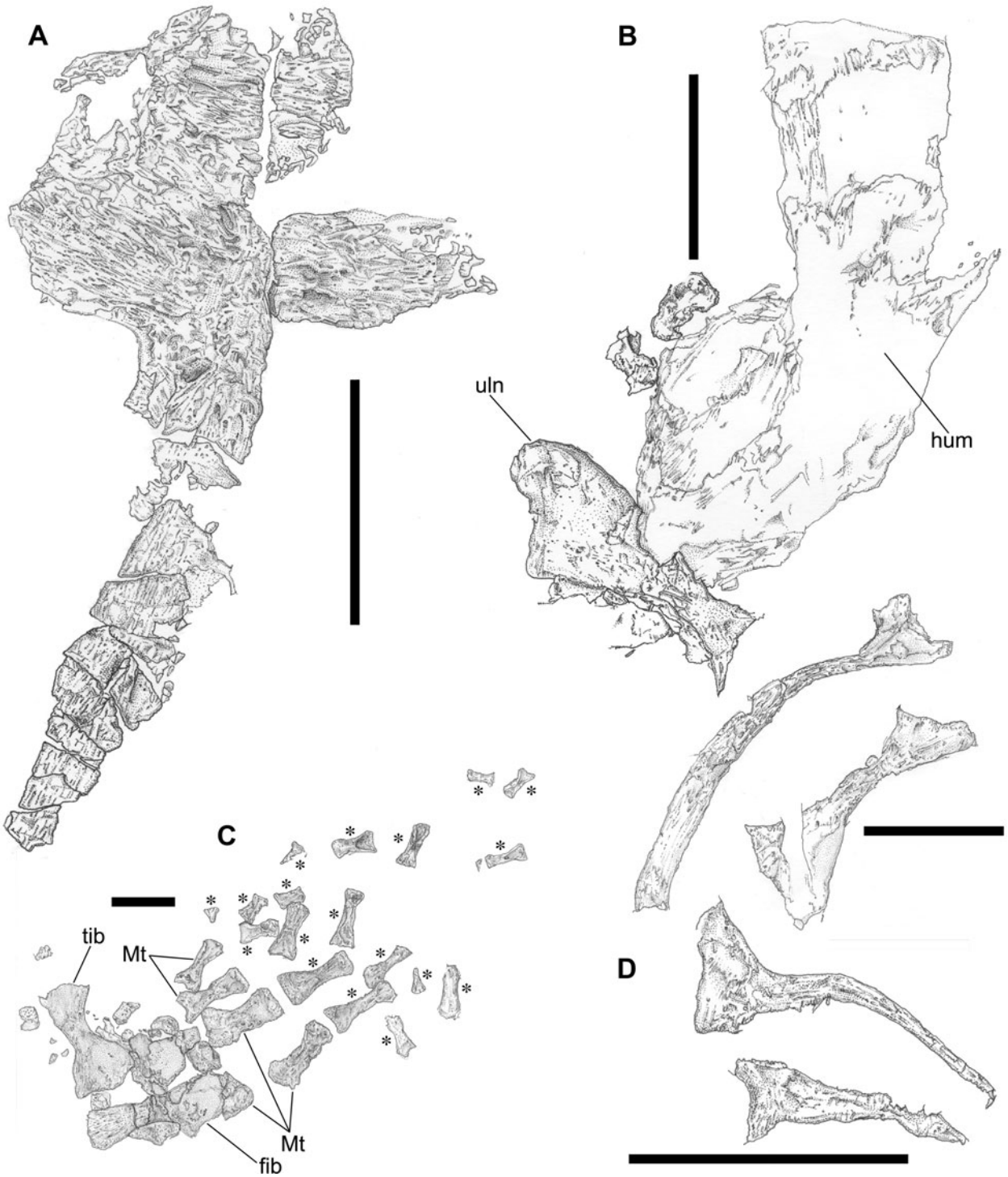

Figure 3 *Eldeceeon rolfei.* (A) Interpretive drawing of interclavicle of NMS G.1990.7.1a (part). (B) Interpretive drawing of humerus and ulna of NMS G.1990.7.1b (counterpart). (C) Interpretive drawing of pes of NMS G.1990.7.1a (part). (D) Interpretive drawing of ribs of NMS G.1990.7.1b (counterpart) showing, from top to bottom, mid trunk, mid cervical, posterior trunk and, possibly, anterior caudal ribs. Abbreviations: fib = fibula; hum = humerus; Mt = metatarsal; tib = tibia; uln = ulna; asterisks indicate phalanges. Scale bars = 10 mm.

ornament is visible on the intertemporal, supratemporal, and tabular, consisting of irregularly spaced low tubercles and sparse low ridges (Fig. 2c). The ornament of the quadratojugal consists, for the most part, of subparallel, elongate, and anastomosed ridges and grooves (Figs 2b, c, 5b, d). The lateral surface of the maxilla shows light longitudinal striations and rugosities intercalated with slender ridges, and is more densely pitted at its anterior extremity (Fig. 2b, c).

3.1.3. Sutural patterns. Despite disruption, several skull roof sutures are traceable (Figs 2c, 5d, 7a–c). Where bones have been dislocated, the partial extension of bone overlap surfaces (underlying lamellae *sensu* Kathe 1999) and adjacent sutural seams are visible (see descriptions of individual bones below). On the skull roof, most sutures are gently sinuous. Slightly more elaborate sutural interdigitations occur between the bones of the central skull roof series (premaxillae; nasals; frontals, parietals; postparietals), both in anteroposterior succession and between antimeres, as well as between postparietals and tabulars and between parietals and tabulars. By contrast, in *Silvanerpeton* most sutures are gently undulating.

3.1.4. Premaxilla. Each premaxilla is divided into a subtriangular upper process and a subrectangular basal portion

https://doi.org/10.1017/S1755691020000079 Published online by Cambridge University Press

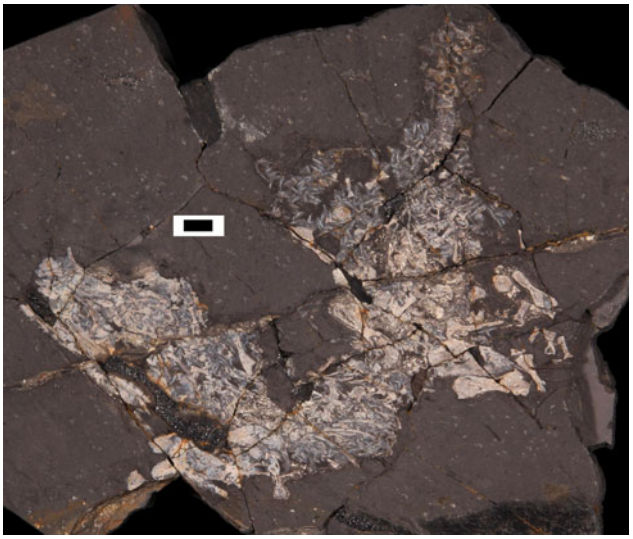

Figure 4 *Eldeceeon rolfei*. Photograph of UMZCT.2013.3a (part). Scale bar = 10 mm.

(Figs 2, 7a–c) delimiting, respectively, the anterior margin and anterior half of the ventral margin of the external nostril. The basal portion includes both maxillary and vomerine processes. The posterodorsally orientated upper process (= 'nasal' process of some authors) contacts its antimere along a weakly sinuous medial suture, and appears comparatively more robust and wider than its homologue in *Silvanerpeton*. Posterodorsally, it forms a strongly interdigitating suture with the nasal. The process widens rapidly ventrally before merging smoothly into the subrectangular basal portion. The abbreviated posterolateral (= 'maxillary') process of the basal portion contacts the anterior extremity of the maxilla along a narrow oblique suture, as in *Silvanerpeton*. Although the posterior (= 'vomerine') process of the basal portion is not visible, it is reasonable to assume it was wide and anteroposteriorly abbreviated, judging from the shape of the anterior extremity of the vomers (Fig. 2b, c), as preserved (see section 3.2.3).

3.1.5. Nasal. The broad, flat, and irregularly subpentagonal nasals (vs narrow, elongate, and rectangular in *Silvanerpeton*) show irregularly indented margins and occupy ~80 % of the length of the skull's preorbital region in dorsal aspect (Figs 2, 5, 7a–c). The conjoined nasals attain their greatest width at the triple sutural junctions with the prefrontals and lacrimals, along a transverse line situated slightly posterior to their mid length. The combined width of the nasals is greater than that of the frontals, unlike in *Silvanerpeton* where these two widths are nearly identical. In our reconstruction (Fig. 7c), the nasals are squat and foreshortened as a result of the slope of the dorsal surface of the preorbital region. However, their actual length would be slightly greater in a full plan view, as shown in NMS G.1990.7.1 (counterpart; Fig. 2c). In UMZC T.2013.3 (Figs 4, 5), both nasals are disrupted but have maintained their mutual spatial relationships. Their lateral margins are divided by an anterior portion in contact with the lacrimal and a posterior portion in contact with the prefrontal (Fig. 7a–c; see also description of lacrimal below).

3.1.6. Frontal. The shape and proportions of the frontals resemble those of *Silvanerpeton*, but differ from the latter in three respects (Figs 2c, 5d, 7c): (1) in both taxa the frontals decrease in width posteriorly, more gradually in *Eldeceeon* than in *Silvanerpeton*, immediately behind the triple sutural joints between frontals, prefrontals, and postfrontals; (2) the combined width of the posterior extremities of the frontals at the level of their sutures with the parietals is proportionally greater in *Eldeceeon* than in *Silvanerpeton*, and occupies more than half of the skull table width at the same transverse inter-orbital level; (3) the centres of ossifications of the frontals in *Eldeceeon* occur slightly posteromedial (anteromedial in *Silvanerpeton*) to the triple sutural joints between frontals, prefrontals, and postfrontals. As reconstructed, the frontals of *Eldeceeon* are only slightly longer than the parietals.

3.1.7. Parietal. The parietals delimit a subcircular pineal foramen (elongate and irregularly sub-elliptical in *Silvanerpeton*) situated slightly anterior to the inter-parietal suture mid length (Figs 2b, c, 5, 7c). The pre-pineal region of each parietal is more regularly trapezoidal than in *Silvanerpeton*, increases more gradually in width anteroposteriorly, and is comparatively wider relative to the width of the skull table at the same transverse level (this is partly due to the shape and proportions of the posterior half of the postfrontal; see section 3.1.13.). The post-pineal region is approximately square, its width changing only slightly as a result of the gentle lateral concavity of the parietal–supratemporal suture. The posterolateral area of each parietal forms a distinctly longer suture with the tabular than in *Silvanerpeton*. Unlike *Silvanerpeton*, *Eldeceeon* does not show a small, posterolateral rectangular 'lappet' wedged between the posteromedial corner of the supratemporal and the anterolateral corner of the postparietal.

3.1.8. Postparietal. The postparietals are comparatively shorter and narrower than those of *Silvanerpeton*. Their maximum width is about half of the width of the parietals along their posterior sutural margins (Figs 2b, c, 7c) and form strongly interdigitating sutures with the tabulars. A narrow, smooth flange extends posterior and, presumably, slightly ventral to the posterior margin of the sculptured dorsal surface of each postparietal. From its mid-point, the flange widens slightly medially before meeting its antimere, as well as laterally where it merges into a similar but narrower flange projecting from the tabular.

3.1.9. Intertemporal. The subquadrangular intertemporals are the smallest bones in the lateral temporal series, unlike in *Silvanerpeton* where they form conspicuous pyriform elements. In *Eldeceeon*, they are slightly longer than wide, with smoothly convex or weakly undulating anterior, mesial, posterior, and lateral margins, and with their greater axis orientated slightly obliquely (Figs 2c, 5d, 7a–c). The anterior extremity of each intertemporal is aligned with the mid-point of the pre-pineal tract of the inter-parietal suture, while the posterior extremity is aligned with the posterior border of the pineal foramen.

3.1.10. Supratemporal. The supratemporals extend anteroposteriorly for the entire length of the post-pineal tract of the inter-parietal suture, attaining their greatest width at the mid-point level of this suture (Figs 2c, 5d, 7a–c). The anterior half of each supratemporal narrows imperceptibly anteriorly, while the posterior half tapers rapidly, forming a blunt squarish posterior extremity. Both the mesial and the lateral margin of the bone are convex, the former more markedly so, and its sutural contact with the tabular is slightly indented. Its shallowly embayed anterior margin accommodates the intertemporal. A key difference between the supratemporals of *Eldeceeon* and those of *Silvanerpeton* is the fact that in the latter taxon, the anterior and posterior margins are anteromedially to posterolaterally oblique.

3.1.11. Tabular. The tabulars wrap around the posterolateral corners of the skull table (Figs 2c, 5d, 7a–c). They are slightly wider than long, with slightly sinuous lateral margins in dorsal aspect. Each tabular forms strongly interlocking sutures with the postparietals and parietals. The lateralmost portion of the anterior margin of the tabular accommodates the posterior extremity of the supratemporal. The posterolateral corner of the bone forms a stout process with a smoothly curved profile, projecting posterior to the level of the postparietal flanges. This process resembles the pitted dorsal portion of the

https://doi.org/10.1017/S1755691020000079 Published online by Cambridge University Press

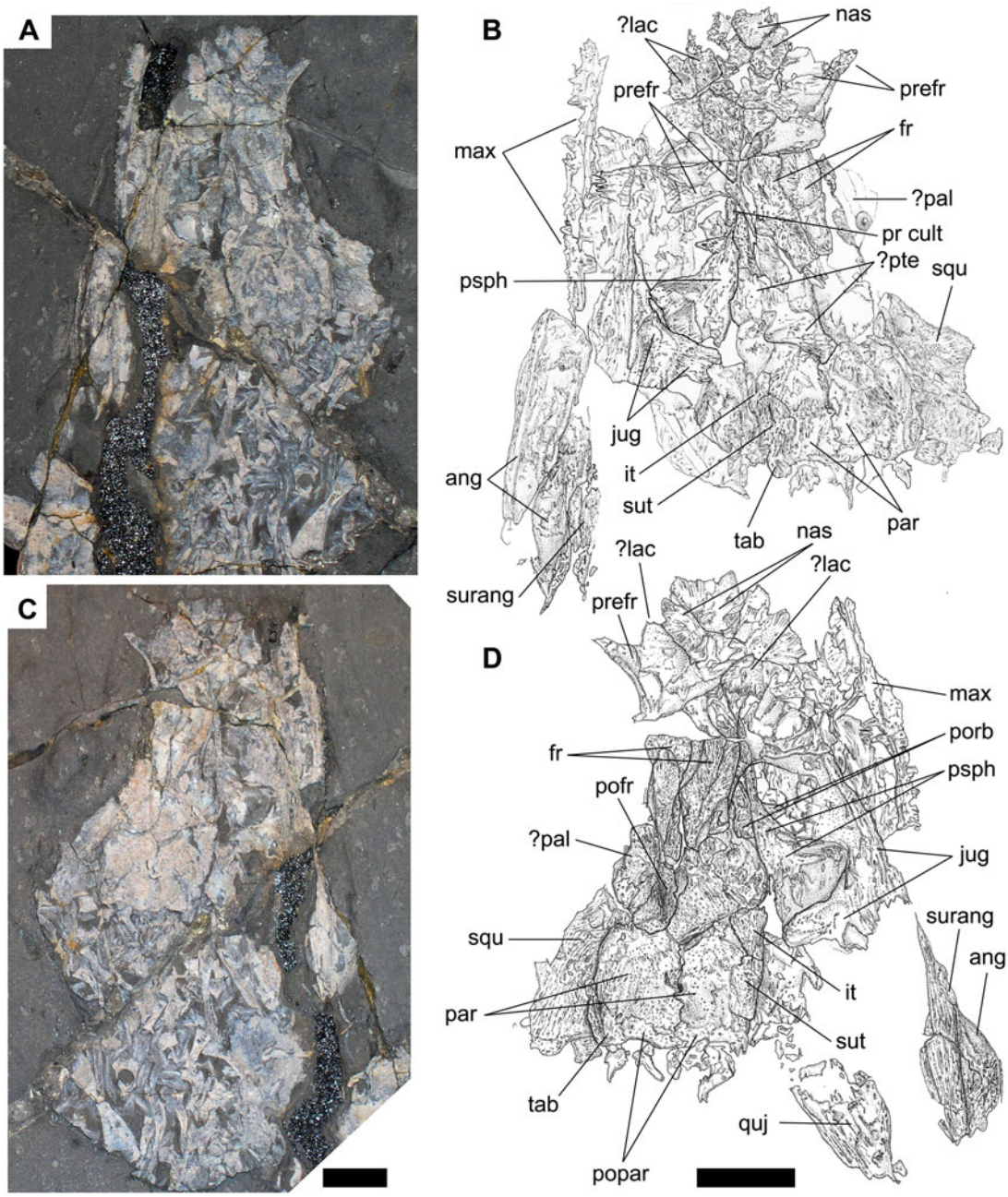

Figure 5 *Eldeceeon rolfei*. (A) Photograph of skull of UMZCT.2013.3a (part). (B) Interpretive drawing of same. (C) Photograph of skull of UMZCT.2013.3b (counterpart). (D) Interpretive drawing of same. Abbreviations: ang = angular; fr = frontal; it = intertemporal; jug = jugal; lac = lacrimal; max = maxilla; nas = nasal; pal = palatine; par = parietal; pofr = postfrontal; popar = postparietal; porb = postorbital; pr cult = cultriform process; preart = prearticular; prefr = prefrontal; premax = premaxilla; psph = basiparasphenoid; pte = pterygoid; quj = quadratojugal; squ = squamosal; surang = surangular; sut = supratemporal; tab = tabular. Scale bars = 10 mm.

tabular horn seen in various anthracosauroids (e.g., Panchen 1970; Holmes 1984, 1989; Clack 1987, 2012; Panchen & Smithson 1988; Klembara 1997; Klembara & Ruta 2004a, 2005a; Ruta & Clack 2006). However, it is not possible to ascertain the presence of a 'subdermal' component of the horn. Immediately mesial to the process, a narrow, smooth, subtriangular flange detaches from the main corpus of the tabular and contacts the postparietal flange along a short oblique suture (Fig. 2c). In all these features, the tabulars of *Eldeceeon* differ from those of *Silvanerpeton*, as follows: (1) the dorsal surface of each tabular in *Silvanerpeton* is less than half of that of the adjacent postparietal – in *Eldeceeon*, the tabulars are distinctly larger than the postparietals; (2) the tabulars of *Silvanerpeton* are plate-like subrectangular elements, longer than wide, without a posterolateral pronounced process, and with a slender, posterolaterally directed, spike-like horn – in *Eldeceeon*, the tabulars are subtriangular, wider than long, with a robust posterolateral process, and no evidence of a subdermal horn, as far as we can ascertain; and (3) in *Silvanerpeton*, the nearly straight posterior margins of the tabulars are obliquely orientated, while their anterior margins are divided into a longer lateral portion and a shorter mesial portion forming an obtuse angle – in *Eldeceeon*, the posterior margins of the tabulars are shallowly concave, while the anterior margins are approximately transversely orientated and irregularly indented.

3.1.12. Prefrontal. The prefrontals contribute to the anterodorsal and most of the anterior sections of the orbital margin (Figs 2b, c, 5b, d, 7a–c). Each consists of a slender, triangular, and posteriorly acuminate ramus (comparatively more robust than that of *Silvanerpeton*) and an anterior, triangular, and fan-like portion (comparatively larger, but otherwise similar to that of *Silvanerpeton*). Along the ramus, the lateral margin of

https://doi.org/10.1017/S1755691020000079 Published online by Cambridge University Press

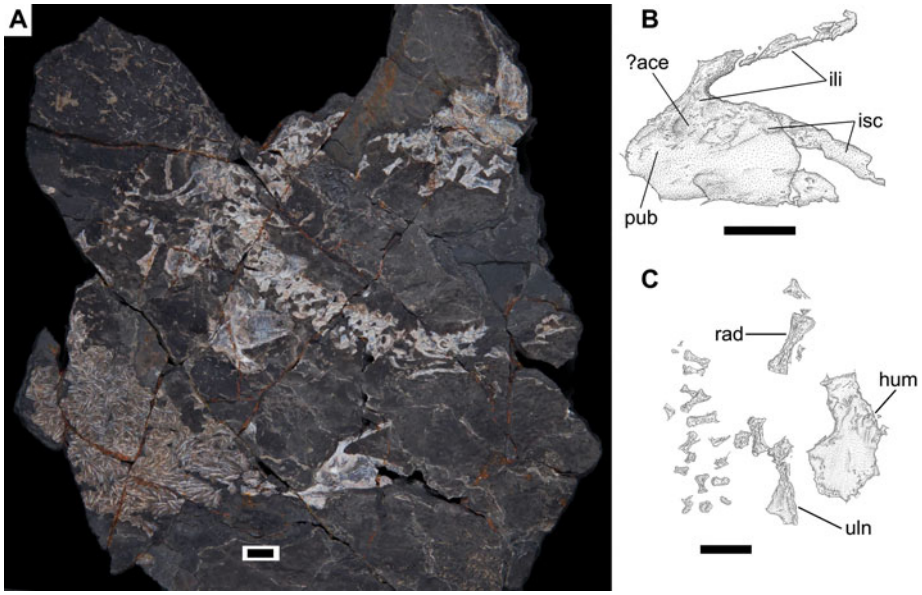

Figure 6 *Eldeceeon rolfei*. (A) Photograph of UMZC T.1350a (part). (B) Interpretive drawing of pelvis of same. (C) Interpretive drawing of forelimb of same. Abbreviations: ace = acetabulum; hum = humerus; ili = ilium; isc = ischium; pub = pubis; rad = radius; uln = ulna. Scale bars = 10 mm.

the prefrontal (sutured with the frontal) is gently curved. More anteriorly, at the transition between the ramus and the fan-like portion, this margin becomes irregularly sinuous up to the level of the triple sutural joint between prefrontal, frontal, and nasal. More anteriorly, the margin zigzags along the sutural contact with the nasal. The fan-like portion widens rapidly anteroventrolaterally, where it contacts the preorbital squama of the lacrimal and contributes to a substantial part of the snout region between the orbit and the external nostril.

3.1.13. Postfrontal. The postfrontals are comparatively narrower than those of *Silvanerpeton* and contribute to the dorsal and part of the posterodorsal orbital margin (Figs 2c, d, 5, 7a–c). Unlike the semi-crescentic postfrontals of *Silvanerpeton*, those of *Eldeceeon* are sickle-shaped, with an anterior, strongly curved, and narrow ramus forming a point contact with the prefrontal and merging gradually into a wider posterior portion. The embayed posterior margin of the bone accommodates the intertemporal. Anterolateral to the embayment, the postfrontal shows a small abbreviated process sutured with the postorbital. At this level, the postfrontal reaches its maximum width, which is comparable with that of the adjacent pre-pineal portion of the parietal. Unlike in *Silvanerpeton*, the postfrontal–parietal suture is gently convex posteromesially. In UMZC T.2013.3 (Fig. 5c, d), the posterior portion of the (presumed) anatomically left postfrontal appears to be stouter and with less strongly curved lateral and mesial margins than its homologue in NMS G.1990.7.1 (Fig. 2c).

3.1.14. Postorbital. The large triangular postorbitals are stockier and proportionally larger than those of *Silvanerpeton*, and contribute to most of the posterior orbital margin (Figs 2c, d, 7a–c). Each consists of an anterodorsal, an anteroventral, and a posterior ramus. The anterodorsal ramus is poorly delimited from the main corpus of the bone and contacts the postfrontal along a short suture. The robust and subrectangular anteroventral ramus is about half as long as the total length of the bone (measured in dorsal or lateral aspects), and forms a slanting suture with the dorsal process of the jugal. This suture is proportionally longer than in *Silvanerpeton*, in which the anteroventral ramus, while distinct, is about one-third of the length of the postorbital. In addition, the anteroventral corner of the ramus extends into a digitiform process in *Eldeceeon* (absent in *Silvanerpeton*). The posterior ramus of the postorbital is comparatively much shorter and narrower than its homologue in *Silvanerpeton* and contacts the lateral margin of the supratemporal a short distance behind the lateral extremity of the intertemporal–supratemporal suture (Fig. 2c). The main corpus of the postorbital is occupied by a distinct longitudinal ridge. Posteriorly, the ridge merges smoothly into the surface of the posterior ramus. It increases slightly in depth anteriorly, before disappearing immediately behind the orbital margin. The ventral part of the ridge marks the dorsalmost portion of the anteroventral process (Fig. 7a–c).

3.1.15. Jugal. The triradiate jugals consist of a dorsal ('postorbital'), an anterior ('suborbital'), and a posterior ramus. Each contributes to a short tract of the posterior orbital margin, as well as to its posteroventral and ventral tracts (Fig. 7a–c). In NMS G.1990.7.1 (Fig. 2c), only a small area of the dorsal ramus of the right jugal is visible, in contact with the right postorbital. In UMZC T.2013.3 (Fig. 5c, d), most of the right jugal is visible in lateral and mesial aspects, except for the rearmost portion, which is largely incomplete. However, this portion can be reconstructed from the morphology of the surrounding elements. The anterior ramus is slender and elongate and contributes to the ventral orbital margin. Its depth is approximately constant in its anterior two-thirds, increases gently in its posterior one-third, and merges smoothly into the corpus of the bone. The dorsal ramus is broad and its posterior margin (in contact with the squamosal) slopes slightly posteroventrally. The posterior ramus is likely to have contributed to the ventral margin of the cheek region, separating the quadratojugal from the maxilla, although only its anteriormost portion is visible. The rest of the ramus is reconstructed as a short triangular flange extending posterior to the maxilla.

3.1.16. Lacrimal. The lacrimals consist of a short, posterior suborbital ramus and an anterior, elongate, subrectangular lamina (Fig. 7a–c). No specimen shows a complete lacrimal, as remnants of this bone are invariably heavily disrupted and dislocated. However, it is possible to put together a composite reconstruction from preserved fragments of the left lacrimal in UMZC T.2013.3 (Fig. 5a, b) as well as from the shape and proportions of adjacent skull bones, particularly the prefrontal and the nasal (Figs 2b, c, 5). As reconstructed, the lacrimal contributes to part of the anterior and the anteroventral orbital margin. The ramus length is approximately one-quarter of the

https://doi.org/10.1017/S1755691020000079 Published online by Cambridge University Press

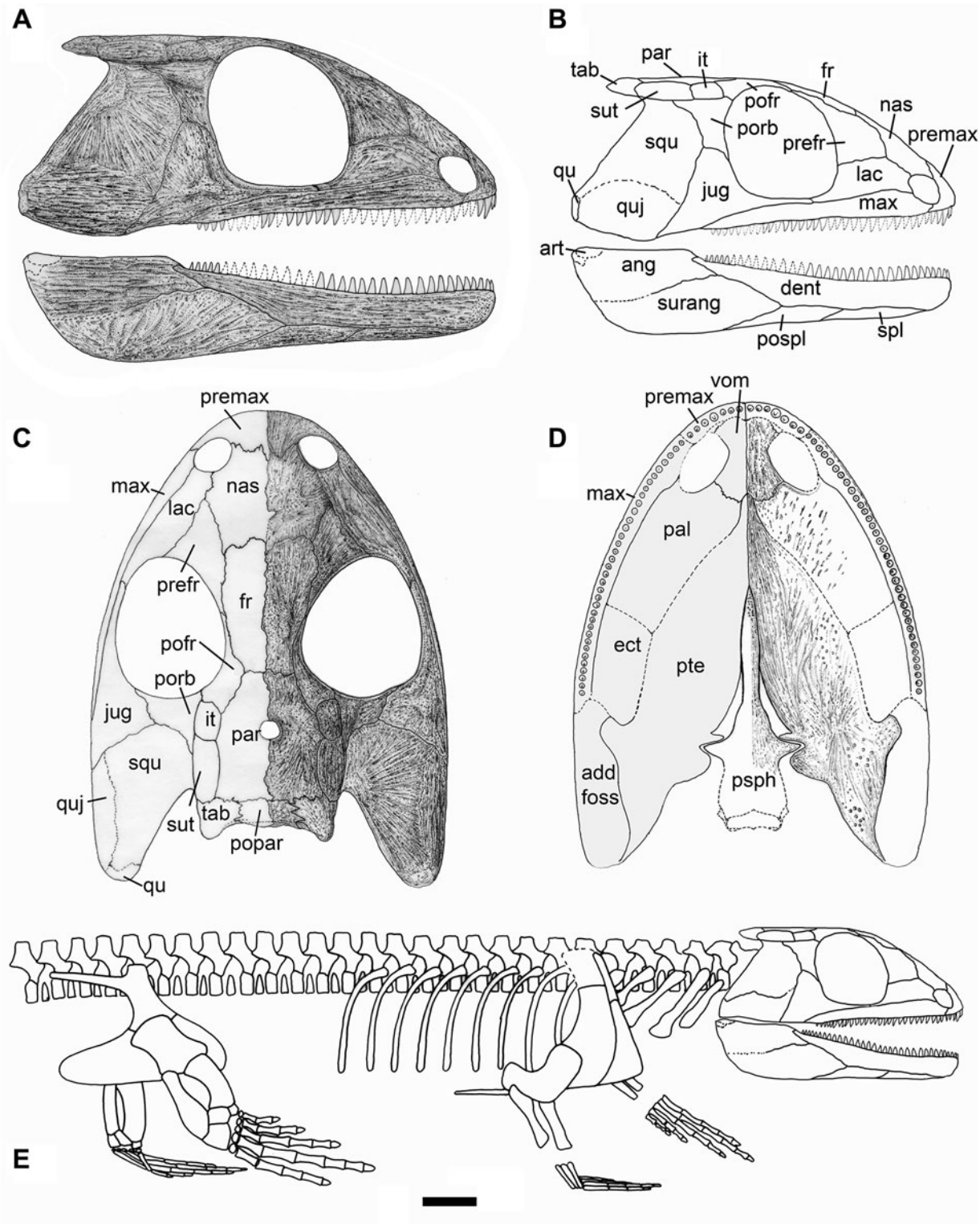

Figure 7 *Eldeceeon rolfei*. (A) Reconstruction of skull and lower jaw in right lateral view. (B) Line drawing of skull in right lateral view, with bones labelled. (C) Skull in dorsal view, with bones labelled on left-hand side of diagram. (D) Skull in ventral view, with bones labelled on left-hand side of diagram. (E) Full skeletal reconstruction. Abbreviations: add foss = adductor fossa; ang = angular; art = articular; dent = dentary; ect = ectopterygoid; fr = frontal; it = intertemporal; jug = jugal; lac = lacrimal; max = maxilla; nas = nasal; pal = palatine; par = parietal; pofr = postfrontal; popar = postparietal; porb = postorbital; pospl = postsplenial; pr cult = cultriform process; preart = prearticular; prefr = prefrontal; premax = premaxilla; psph = basiparasphenoid; pte = pterygoid; qu = quadrate; quj = quadratojugal; spl = splenial; squ = squamosal; surang = surangular; sut = supratemporal; tab = tabular; vom = vomer. Scale bar = 10 mm.

maximum orbit length, and deepens rapidly anteriorly before merging with the lamina, as in *Silvanerpeton*. The lamina contributes to the posterior margin of the external nostril and appears to be comparatively less deep than the lamina of *Silvanerpeton*. The shape and size of the prefrontal and nasal suggest that the dorsal margin of the lamina consisted of a shorter anterior tract and a longer posterior tract meeting at an obtuse angle. The ventral margin, in contact with the maxilla, probably showed a small anterior embayment corresponding to a 'peak' in the anterior part of the upper margin of the maxilla (see section 3.1.19). Overall, the lamina is less deep and with a less rounded dorsal margin than that of *Silvanerpeton*.

https://doi.org/10.1017/S1755691020000079 Published online by Cambridge University Press

3.1.17. Squamosal. The subtrapezoidal squamosals are substantial bones (Figs 1, 2b, c, 7a–c). The anterior extremity of each squamosal (at the triple sutural joint between squamosal, postorbital, and jugal) reaches anteriorly almost to the level of the intertemporal mid length. Its posteroventral corner (in lateral aspect) projects distinctly behind the transverse level of the posterolateral processes of the tabulars. The posterior free margin of the squamosal forms an angle of ~53 degrees with the horizontal and is mostly straight except in its dorsalmost tract, where it produces a small shallow embayment immediately below the skull table. At this level, the bone reaches as far posteriorly as the posteriormost part of the supratemporal. However, there is no evidence that the squamosal of *Eldeceeon* contacted the tabular, unlike in *Silvanerpeton*. Along its dorsal margin, below the lateral temporal series, the squamosal shows a longitudinal thickening representing the lateral border of the articulation surface between the cheek and the skull table, possibly suggesting the presence of a hinge-like suture (Panchen 1970; Smithson 1985; Clack 1987). In NMS G.1990.7.1, the ventralmost part of the posterior margin of the squamosal shows a curious depressed area seemingly devoid of dermal sculpture (Fig. 2c), which probably accommodated a small process from the quadratojugal in life. Along the course of the posterior margin, the surface of the squamosal forms a shallow and smooth flange delimited by an anterior ridge.

3.1.18. Quadratojugal. Although the quadratojugals are only partially preserved (Figs 1, 2b, c, 5), it is possible to reconstruct their posterior profile and most of their lower margin in lateral aspect (Fig. 7a–c). However, the course of the quadratojugal–squamosal suture, only partly visible in the holotype (Fig. 1), and the spatial relationship between the anteriormost part of the quadratojugal and the posterior ramus of the jugal are largely conjectural. The quadratojugal contributes to more than one-third of the depth of the posterior area of the suspensorium. Its ventral margin is smoothly convex and projects slightly below the level of the rearmost portion of the maxilla. Its anteriormost part is estimated to have extended approximately to the level of the posterior process of the postorbital in lateral view. Its short posterodorsal margin is in continuity with the squamosal free margin, and the transition between the two bones at this level is marked by a subtle change in slope. Below this slope, the quadratojugal terminates in a blunt squarish extremity presumably abutting against, and partially wrapped around, the lateral surface of the quadrate (Fig. 7c). As reconstructed, the quadratojugal of *Eldeceeon* appears deeper and more robust than in *Silvanerpeton*.

3.1.19. Maxilla. The shape of the maxilla conforms to that of most other early tetrapods (Figs 2b, c, 5, 7a–c). Its upper and lower margins converge towards one another anteroposteriorly. Its anterior margin is shallowly concave and contributes to the posterior half of the ventral margin and to the lower half of the posterior margin of the external nostril. The border for the nostril is visible in NMS G.1990.7.1 (Fig. 2c). The deepest part of the maxilla occurs slightly posterior to the nostril, where the upper margin of the bone shows a low triangular 'peak'. Posterior to this level, the upper margin has a nearly straight profile, sloping slightly posteroventrally to a point situated below the mid-length of the suborbital process of the jugal. Posterior to this point, the upper margin shows a more pronounced slope such that the maxilla decreases rapidly in depth. A further change in slope is visible more posteriorly, aligned vertically with the posterior margin of the orbit. Behind this point, the maxilla forms an acuminate triangular process separated from the quadratojugal. *Silvanerpeton* differs from *Eldeceeon* in that the upper margin of its maxilla is nearly straight.

3.2. Palate

3.2.1. General features. Comparisons between the palates of *Eldeceeon and Silvanerpeton* are limited due to incomplete preservation in the former taxon (except for the pterygoid and the vomer; Figs 2b, c, 7d). Most likely, the palate was either closed or exhibited narrow vacuities, and some mobility may have characterised the palate–braincase junction (e.g., Panchen 1970; Smithson 1985; Clack 1987).

3.2.2. Pterygoid. NMS G.1990.7.1 (Fig. 2b, c) supplies most of the information on the pterygoid. Combined data from the part and counterpart of this specimen suggest that the pterygoid has a proportionally more gracile palatal ramus and a more abbreviated quadrate ramus than its homologue in *Silvanerpeton*. The palatal ramus is vaguely lanceolate. Anteriorly, it terminates in a narrow triangular process in contact with its antimere along a straight line. The full anteroposterior extension of this contact is estimated to have been less than one-third of the projected length of the entire palatal ramus in ventral aspect. This is indicated by a gentle change in the curvature of the mesial margin of the ramus, which parts from its antimere to follow a smoothly convex course and continues to the level of the anterior process of the basipterygoid recess (Fig. 2c). Here, the margin turns abruptly mesially, resulting in the occurrence of a deep notch in the profile of the ramus. The deep basipterygoid recess has a narrow, sub-elliptical, and asymmetric profile. It is delimited by a gracile anterior process shaped like a thin bony sliver and a sturdier, mesiolaterally shorter, and subtriangular posterior process (Fig. 2c). The lateral margin of the palatal ramus is visible only in part, and the precise nature of its sutural contact with the palatine and ectopterygoid cannot be reconstructed. The quadrate ramus forms a triangular flange tapering rapidly posteriorly, and with a smoothly convex mesial margin and a semiparabolic lateral margin. Its proportions suggest that the adjacent subtemporal fossa of *Eldeceeon* would have been comparatively much smaller than that of *Silvanerpeton*. The anterior extremity of the lateral margin turns sharply laterally to produce a distinct, subrectangular lateral flange (Fig. 2c). This flange would have conferred a constriction to the anterior profile of the subtemporal fossa, but it is unclear whether a substantial anterior extension of the fossa was present lateral to the ectopterygoid. Preservation makes it impossible to ascertain whether the pterygoid contacted an internal process of the jugal ('insula jugalis' *sensu* Bystrow & Efremov 1940), such as is observed in *Silvanerpeton*. Despite diagenetic compression of the quadrate ramus, there is no evidence of a transverse flange along the area where the quadrate ramus continues onto the corpus (Fig. 2c).

3.2.3. Vomer. Both vomers are preserved (Fig. 2b, c). Although they are visible in dorsal and ventral aspect, their exposed surfaces are almost featureless, except for a number of irregular longitudinal striations and shallow grooves. Toothless vomers occur in other anthracosaurs and have at times been regarded as a characteristic feature of this group (e.g., Panchen 1970), although exceptions are known (e.g., *Silvanerpeton*; Ruta & Clack 2006). The elongate and subrectangular vomers of *Eldeceeon* have nearly straight mesial margins and shallowly concave lateral margins forming most of the lateral choanal border. Their irregularly sinuous posterior margins are orientated slightly obliquely (anterolaterally to posteromesially). In this feature, they differ from the vomers of *Silvanerpeton*, which terminate in robust triangular projections flanking the anterior part of the mesial margins of the palatines. In *Eldeceeon*, the anteriormost extremities of the palatal rami of the pterygoids were probably wedged between the posteromesial corners of the conjoined vomers in life. The spatulate anterior extremity of each vomer

https://doi.org/10.1017/S1755691020000079 Published online by Cambridge University Press

would have been appressed against the internal surface of the basal portion of the premaxilla.

3.2.4. Palatine. Fragments of the left and right palatines are visible in NMS G.1990.7.1 (Fig. 2b, c), allowing us to reconstruct the anteriormost part of the palatine including the course of the choanal border. The palatine probably occupied a substantial proportion of the palatal surface, but its orientation and proportions remain largely conjectural. The choanal margin is subsemicircular. On the ventral side, a sharp straight ridge occurs adjacent to the mesial part of this border. This ridge runs anteromedially to slightly posterolaterally, widening slightly and becoming increasingly sharper posteriorly, before merging into the preserved part of the surrounding surface of the bone. Irregular rugosities and depressions are visible on the larger of the two palatine fragments in NMS G.1990.7.1.

3.2.5. Ectopterygoid. No preserved bony fragment can be convincingly assigned to the ectopterygoid, as the relevant region of the palate is covered by the lower jaw rami (but see comments on the palatal dentition). As in the case of the palatine, the ectopterygoid would have formed a substantial rectangular plate, based upon general skull proportions.

3.2.6. Quadrate. A small, subrectangular bony fragment immediately posterior to, and partly overlapping, the posterior extremity of the quadratojugal in NMS G.1990.7.1 (Fig. 2b, c) is interpreted as a partially preserved quadrate. Its surface is almost featureless, except for the occurrence of weak elongate rugosities. The direction of its greatest elongation may correspond to the dorsoventral orientation of the bone, but no other details are visible.

3.3. Braincase

Most of the parabasisphenoid complex anterior to, and including, the basipterygoid processes can be reconstructed with accuracy (Figs 2b, c, 7d). However, only small disrupted fragments of the basal plate are visible. The cultriform process of the parasphenoid is parallel-sided for most of its length, and extends for approximately two-thirds of the projected length of the palatal rami of the pterygoids. Its anterior extremity, visible in NMS G.1990.7.1 (counterpart) appears broken off and is visible in close proximity to the rest of the process (Fig. 2c). This broken extremity is considerably narrower than the rest of the cultriform process, and has a lanceolate profile rapidly tapering to a point anteriorly. It is possible that a short section of the process, between the broken margin and the anterior extremity, is missing. As reconstructed, the process is likely to have been accommodated, at least in part, along a narrow space between the mesial margins of the palatal rami of the pterygoids. This is based upon the fact that the broken off extremity carries a small irregular patch of denticles arranged along a narrow longitudinal strip of its exposed surface. Immediately anterior to the basipterygoid processes, the cultriform process widens slightly (Fig. 2b, c). This area of the parabasisphenoid complex is slightly disrupted and partially covered by skull roof bones. The basipterygoid processes are robust and with a subparabolic profile as preserved.

3.4. Lower jaw

Although no specimen shows complete lower jaw rami, it is possible to provide a clear picture of their general proportions and details of the sutural contact among their constituent bones (Figs 2b, c, 5, 7a, b). Both jaw rami are exposed in lateral view in NMS G.1990.7.1, and the holotype shows the posterior extremity of the right ramus (Fig. 1). The lower jaw is slightly more robust than that of *Silvanerpeton*, and reminiscent of the jaws of various discosauriscid seymouriamorphs (e.g., Klembara 1997; Klembara & Ruta 2004a, 2005a). Similarities involve a blunt-ended, squarish posterior extremity (in lateral view), a smoothly curved and subsemicircular profile of the anterior extremity, and the fact that the ramus increases in depth gradually from its anterior extremity to the posterior end of the dentigerous portion of the dentary. The angular region is comparatively deeper and with a more strongly convex ventral margin in lateral aspect than in discosauriscids, and the surangular crest is proportionally smaller and with a 'step-like' profile. There are no traces of lateral line canals.

3.4.1. Dentary. The dentary is ~70 % as long as the ramus (Fig. 2b, c, 7a, b). In lateral aspect, its anterior margin is smoothly convex. Its upper margin is very shallowly concave in its anterior half, but nearly straight and sloping gently posterodorsally in its posterior half. Combined information from the preserved portions of the upper margins of the infradentaries suggests that the ventral margin of the dentary shows a sudden change in slope at the triple sutural joint between dentary, angular, and postsplenial. Anterior to this joint, the depth of the bone is approximately constant, whereas posterior to it, it decreases rapidly. Posterior to the triple sutural joint between dentary, surangular, and angular, the dentary forms a finger-like projection extending slightly posterior to the last dentary tooth and appressed against the surangular, immediately anteroventral to the surangular crest.

3.4.2. Splenial and postsplenial. The extent of the lateral exposure of these two bones, such as is observed in NMS G.1990.7.1 (Fig. 2b, c, 7a, b), may have been exaggerated by compaction. However, it is clear that both contribute to a significant proportion of the projected lateral aspect of the ramus, and are approximately equal in length. The splenial is a narrow sliver of bone, narrowing gently to a point immediately behind the anterior extremity of the dentary and forming a nearly straight suture with the dentary, in continuity with the dentary–postsplenial suture. The lateral projection of the postsplenial is deeper than that of the splenial. Its depth increases slightly from the level of the splenial–postplenial suture to the level of the triple sutural joint between dentary, angular, and postsplenial, situated at the mid length of the postsplenial. Posterior to this level, the postsplenial decreases gradually in depth. The rearmost part of its lateral surface is aligned vertically with the triple sutural junction between dentary, surangular, and angular.

3.4.3. Angular. Most of the lateral surface of the angular (Fig. 2b, c, 7a, b) is visible, except for a small portion of its sutural contact with the surangular. The bone is deepest at the level of its triple sutural junction with the dentary and the surangular. Anterior to this point, the anterodorsal margin of the bone slopes sharply, anteroventrally forming an irregularly convex suture with the dentary. Its posterodorsal margin slopes gently posteroventrally. Its ventral margin of the angular is divided into a smoothly convex posterior half continuing seamlessly into the posterior margin of the surangular, and a nearly straight anterior half.

3.4.4. Surangular. Despite uncertainties concerning the precise course of its ventral margin, most of the surangular can be reconstructed (Figs 1, 2b, c, 7a, b). It is a sturdy subtrapezoidal bone increasing slightly in depth anteroposteriorly, with a gently convex posterior margin and a nearly straight upper margin. The anterior extremity of the upper margin ends in a small but distinct 'step'-like surangular crest, immediately dorsal to the rearmost extremity of the dentary. A horizontal strip of the lateral surface of the surangular, immediately below the dorsal margin of the bone and extending for about one-fourth of its greatest depth, shows a poorly pronounced sculpture and is likely to have accommodated the internal surface of the quadratojugal in life (see Klembara 1997).

3.4.5. ?Prearticular. In the middle one-third of the left ramus of NMS G.1990.7.1 (Fig. 2b, c), the lower jaw bones appear to be dislocated. Within the gap resulting from

https://doi.org/10.1017/S1755691020000079 Published online by Cambridge University Press

disruption, an irregularly striated bony surface, presumably in mesial aspect, is visible. This surface is tentatively interpreted as belonging to the prearticular, but no salient features can be seen.

Coronoids cannot be observed in any specimen.

3.5. Dentition

The upper and lower marginal dentition is reasonably well preserved, though for most teeth only the outlines of their crowns and, occasionally, their pulp cavities can be discerned (Figs 2b, c, 5, 7a, b, d). The marginal teeth are subconical, with a shallow concave posterior margin in side view, a slightly more pronounced convexity along their anterior margin, and an acuminate tip. The teeth change slightly in size along the maxillary and dentary arcades, but are otherwise uniform in proportions. The premaxilla shows six or seven teeth. In the fully exposed and displaced (possibly left) premaxilla of NMS G.1990.7.1 (Figs 2b, c), the three most anterior teeth appear iso-dimensional, and the height of their crowns is comparable to the depth of the directly overlying basal portion of the premaxilla (see description above). The fourth tooth is nearly twice as large as the anteriormost teeth and more strongly curved. A narrow space is visible immediately posterior to this tooth, but we are unable to ascertain whether it represents the position occupied by a fifth tooth or whether it results from disruption. Behind this space are two more teeth. The more anterior (fifth or sixth) of these two teeth is only marginally smaller than the fourth tooth but with a similar profile. The more posterior tooth (sixth or seventh) is distinctly smaller and comparable in size to the three most anterior teeth. We estimate that the maxilla housed ~30 teeth (including empty tooth socket positions), but a precise count is difficult because several teeth are missing or broken, and the maxillary arcade is disrupted. Similar difficulties are encountered with estimates of the dentary tooth count. The size difference between the most anterior dentary teeth that we could observe and the middle dentary teeth is less marked than the difference between the middle dentary teeth and the most posterior dentary teeth. There is no appreciable size difference between the largest preserved upper and lower marginal teeth.

There are only glimpses of the palatal dentition. As mentioned in the description of the parabasisphenoid complex (see section 3.3.), the tapering anteriormost extremity of the cultriform process bears a scatter of small denticles arranged in a longitudinal strip in the middle of its ventral surface. It is possible that denticles where present further posteriorly along the cultriform process, but no information is available. Isolated denticle patches are also present on the pterygoids, but it is not possible to ascertain what proportion of the ventral surface of these bones was denticulated. In NMS G.1990.7.1 (Fig. 2c), widely spaced denticles occupy a mediolaterally orientated, narrow strip where the quadrate ramus merges into the corpus of the pterygoid, as well as on a small irregular area situated mesial to its subrectangular lateral flange. Very few scattered denticles are also present on the flange. Finally, widely spaced denticles are visible on the palatal ramus, in particular on its lateral half, almost at the same transverse level as the basipterygoid articulation. Isolated denticles may be present further anteriorly but are much more difficult to discern. No obvious denticles have been found associated with bones of the lateral palatal series. However, both part and counterpart of NMS G 1990.7.1 (Fig. 2c) show two large broken tooth crowns that appear to perforate the surface of a bony element (presumed prearticular; see section 3.4.5.) visible through the dislocated bones of the left jaw ramus. These teeth may represent either palatine or ectopterygoid fangs. A large tooth crown with a subcircular base, in proximity to a heavily worn bone surface, is observed in the counterpart of UMZC T.2013.3, some distance from the preserved right half of the skull roof (Fig. 5a, b), and is likewise tentatively interpreted as a palatal fang.

3.6. Axial skeleton

The full skeletal reconstruction of *Eldeceeon* (Fig. 7e) is based on the three most complete specimens (Figs 1, 2a, 4). It summarises all the available information on the postcranial skeleton. It includes 24 presacral vertebrae, places the scapulocoracoid around vertebra seven, and shows a manual phalangeal formula of 2-3-4-5-4 and a pedal phalangeal formula of 2-3-4-5-4. The carpus is unossified, but the tarsus includes fibulare, tibiale, intermedium, and five distal tarsals. No centralia have been identified. Well-ossified cervical and trunk ribs are shown on the first 14 vertebrae. Very poorly ossified ribs between rib 14 and the pelvis, noted in the text, are illustrated separately (Fig. 3d). The new reconstruction differs from that in Smithson (1994) in having a horizontal presacral vertebral column, the shoulder girdle occupies a slightly more anterior position, and a fully ossified pubo-ischiadic plate is included.

Smithson's (1994) account of the vertebral column of *Eldeceeon* does not require a full redescription, and only a summary of major distinguishing features is given below. The ribs vary in shape and proportions from the cervical to the trunk regions (Fig. 3d), with cervical ribs marked by expanded and triangular distal ends, more robust shafts, and weakly pronounced or no curvature, and trunk ribs marked by a narrow and gently curved profile. All ribs show a distinctly expanded proximal extremity but poor evidence of separation between capitulum and tuberculum. A key issue concerns the proportion and distribution of the trunk ribs, a unique characteristic of *Eldeceeon* (Smithson 1994). Information from the new specimens confirms, to a large extent, Smithson's (1994) observations based upon the holotype and NMS G.1990.7.1 (Figs 1, 2a). Data from UMZC T.2013.3 (Fig. 4) and UMZC T.1350 (Fig. 6) are less easy to interpret, as only a few ribs are visible. A small number of unequivocal trunk ribs are preserved near the posterior region of the heavily disrupted vertebral column of UMZC T.1350 (Fig. 6), but it is unclear whether these occur in a natural position or whether they have been displaced from a more anterior position. In UMZC T.2013.3 (Fig. 4), observations are complicated by the fact that the posterior half of the specimen shows a chaotic arrangement of appendicular, axial, and ventral dermal elements. Although unequivocal trunk ribs are visible, an exact count of these is not possible. A further complication is the fact that in most specimens, slender rib-like elements with a geniculated shaft, an expanded head, and a pointed end (Fig. 3d) are visible in places in the posteriormost trunk region. If indeed these are ribs, we are left with a possible alternative explanation for the peculiar configuration of the axial skeleton of *Eldeceeon*, namely that it did possess a full complement of trunk ribs – longer and more strongly curved anteriorly (an autapomorphic trait, as far as we can tell and in agreement with the original description), shorter and geniculate posteriorly – but that such ribs did not show any gradation in morphology and proportions between those two regions (see also discussion of possible functional interpretation in section 5.1.).

3.7. Appendicular skeleton

3.7.1. Pectoral girdle. We limit our description of the pectoral girdle to a few salient features of the interclavicle only. For further details, see Smithson (1994). Particularly noteworthy is its shape, which readily distinguishes *Eldeceeon* from *Silvanerpeton*. In *Silvanerpeton*, the subrhomboidal anterior ventral plate of the interclavicle transitions smoothly into the elongate triangular parasternal process (Ruta & Clack 2006, fig. 10a) In *Eldeceeon*, the broadly fan-shaped anterior ventral plate is sharply delimited from the narrow and rod-like

https://doi.org/10.1017/S1755691020000079 Published online by Cambridge University Press

parasternal process (Figs 1, 2a, 3a, 4). Although incomplete in UMZC T.2013.3 (Fig. 2a, 6), the interclavicular plate shows a large, sub-elliptical, posterior sculptured region, the surface of which shows irregular depressions, pits, ridges, and grooves. In this specimen, the anterior fringe projecting anteriorly from the smoothly convex anterior margin of the sculptured region is not preserved. The fringe, visible in the holotype (Fig. 1) and in NMS G.1990.7.1 (Fig. 2a), consists of straight radiating ridges separated by narrow sulci, and extends for approximately the same length as the sculptured region, becoming increasingly narrower laterally. The posterolateral margins of the sculptured regions are gently sinuous, with a lateral convexity and a medial concavity, and turn sharply posteromesially at the transition between the plate and the parasternal process. There is some evidence that, immediately behind this point, the anteriormost part of the parasternal process is wide and robust but tapers smoothly posteriorly, such that its straight lateral margins converge, gently posteriorly terminating in a narrowly spatulate end. The ventral surface of the process shows a delicate sculpture of fine striations and pits. The morphology of the interclavicle is unique among anthracosauroids, as far as we can tell, but does bear some similarities with the interclavicles of *Ichthyostega* (Jarvik 1996), *Westlothiana* (Smithson *et al*. 1994), possibly *Solenodonsaurus janenschi* (Carroll 1970; Laurin & Reisz 1999; Danto *et al*. 2012), and especially seymouriamorphs such as *Seymouria baylorensis* (White 1939), *Discosauriscus austriacus* (Klembara & Bartík 2000), *Utegenia shpinari* (Klembara & Ruta 2004b), and *Ariekanerpeton sigalovi* (Klembara & Ruta 2005b). In several seymouriamorphs, in particular, the parasternal process is elongate and often with parallel sides, and merges into a fan-shaped or rhomboid interclavicular plate. However, it often terminates in a fringe-like extremity consisting of 'splayed-out', small digitiform processes. In addition, a 'swelling' occurs in the anterior part of the process.

3.7.2. Fore limb. The humerus was thoroughly described by Smithson (1994), based mostly upon NMS G.1990.7.1. A few additional remarks are provided here using information from UMZC T.1350. Although the humeri of NMS G.1990.7.1 and UMZC T.1350 (Figs 2a, 3b, 6a, c) appear slightly different, this is mostly due to incomplete preservation, which also prevents detailed observation of surface features, including processes and crests (but see remarks on possible ectepicondylar ridge below). In both specimens, part of the anterior portion of the bone and the anteriormost part of the humeral head are heavily disrupted. Each humerus shows a conspicuous and elongate proximal half with a stout and moderately elongate shaft, similar to the condition in *Silvanerpeton*. The posterior margin of the shaft is gently convex in its proximal two-thirds and slightly concave in its distal one-third. Its course slants slightly anterodistally before turning sharply posteriorly along a short, narrow curved edge, marking the transition to the proximal margin of the entepicondyle. This transition is smoother and comparatively broader in UMZC T.1350 (Fig. 6a, c). The entepicondyle forms a distinct subrectangular flange, conferring the well-known L-shaped profile to the humerus, such as is observed in various other early tetrapods (Clack 2012). There is no clear evidence of an ectepicondylar ridge in any of the preserved humeri, certainly as a result of preservation, although a poorly preserved thickening appears just distal and slightly anterior to the point where the posterior margin of the shaft and the proximal margins of the entepicondyle converge in NMS G.1990.7.1 (Fig. 2a). The thickening can be followed for a short distance distally, before it disappears in the central part of the extensor surface of the entepicondylar flange. In UMZC T.1350, there is some evidence of a shallow sub-elliptical depression close to the anteriormost part of the posterior margin of the entepicondyle, in the position that would normally be occupied by the entepicondylar foramen (see also discussion in Ruta & Clack 2006 and Smithson & Clack 2018). However, whether the depression in question does correspond to a poorly preserved foramen remains a moot point. Most of the above observations are based upon NMS G.1990.7.1. The entepicondyle of UMZC T.1350 is partially preserved, presumably missing some of its posterior and posterodistal portions. In the development of a substantial shaft and in the outline and proportions of the entepicondyle, the humerus of *Eldeceeon* resembles closely those of *Archeria* and *Proterogyrinus* (Romer 1957; Holmes 1984, 1989), as well as some of the tetrapod humeri from the Tournaisian of Horton Bluff in Nova Scotia (Anderson *et al*. 2015), but differs somewhat from the best preserved humerus in *Silvanerpeton*, such as was described by Ruta & Clack (2006, fig. 10b).

The radius is poorly preserved in most specimens. In the holotype (Fig. 1), the outlines of the radii are almost complete but poorly discernible from the surrounding matrix. The best-preserved radius is observed in UMZC T.1350 (Fig. 6a, c). As preserved, it does not show obvious features that distinguish it from the radii of other anthracosauroids, although it is broadly similar to that of *Archeria*. The bone has a typical 'dumbbell'-like profile, with expanded extremities and a robust shaft. The overall morphology of the bone conforms to the description provided by Panchen (1970, p. 34) for the radius of *Archeria*, which is similar to that of *Eldeceeon*: '… a flattened cylinder with expanded ends bearing terminal articular surfaces; the one for the humerus being roughly circular, that for the carpus somewhat dorsoventrally [*sic*] flattened, i.e. in the extended horizontal position.'

Ulnae are observed in all specimens (Figs 1, 2a, 3b, 4, 6a, c), albeit in various degrees of completeness and preservation. In the best-preserved examples (UMZC T.2013.3 and T.1350; Figs 4, 6a, c), the bone is characteristically slender (conforming mostly to the generalised anthracosauroid pattern) and, unlike its homologue in *Silvanerpeton* (Ruta & Clack 2006, fig. 6a, c), it exhibits a remarkably robust olecranon process. In its general proportions, the ulna of *Eldeceeon* resembles those of *Archeria* (Romer 1957; Holmes 1989) and *Westlothiana* (Smithson *et al*. 1994.), but is unlike that of *Proterogyrinus* (Holmes 1984), in which the bone appears sturdy and with a less pronounced olecranon process. The best-preserved ulna occurs in UMZC T.2013.3 (Fig. 4). In this specimen, the olecranon process is subparabolic in lateral aspect, with a smoothly curved proximal margin, a gently but distinctly convex posterior margin, and an imperceptibly concave anterior margin sloping anteroventrally before merging into the proximal extremity of the ulna. The distal margin of the ulna slants considerably and is divided into a small, posteroventrally straight segment presumably articulating with the ulnare, and a slightly longer, oblique, and irregularly sinusoidal anterior segment presumably articulating with the intermedium (Figs 1, 4, 6a, c).

For a complete description of the anterior autopod, the reader is referred to Smithson (1994). However, the heavily disrupted autopod of UMZC T.1350 (Fig. 6a, c) shows 21–22 elements of the manus. Only some of these show a reasonably complete outline and they add little additional information to the pattern of bones in the manus. Terminal phalanges (unguals) are represented by two or three triangular elements with concave sides and pointed distal extremity. These do not show any evidence of the lateral flange-like expansions documented in the pedal unguals of *Silvanerpeton* (Ruta & Clack 2006, fig. 10d).

3.7.3. Pelvic girdle. Combined information from all specimens provides a nearly complete picture of the morphology of the pelves (Figs 1, 2a, 4, 6a, b). In general proportions, they resemble those of *Silvanerpeton*, except that in that animal, the pubis appears unossified. By contrast in *Eldeceeon*, the pubo-ischiadic plates are fully ossified in some specimens and show

https://doi.org/10.1017/S1755691020000079 Published online by Cambridge University Press

complete peripheral margins. The ilium consists of two major parts: a compact ventral corpus that sutures with the puboischiadic plate, and a robust neck that connects the corpus to a stout dorsal blade and an elongate post-iliac process.

The outline of the dorsal blade varies slightly in different specimens, but some of this variation reflects, in part, disruption and/or incomplete preservation. Its morphology appears to be unique, certainly among anthracosauroids, as far as we can tell. In the holotype (Fig. 1), the blade shows a complete outline, as reconstructed in Smithson (1994). In this specimen, the transition between the anterior margin of the neck and the anterior edge of the blade is marked by a subtle change in curvature, such that the lowermost part of the edge of the blade detaches from the margin of the neck following a short vertical tract, before turning sharply posterodorsally. From this point, the anterior edge of the blade is nearly straight and can be followed along an oblique direction up to the dorsalmost point of the blade. The latter forms a small, blunt-topped, subtriangular 'peak'. From the 'peak', the margin of the blade continues posteroventrally, forming a shallow embayment dorsally followed by a broadly convex tract more ventrally, followed, in turn, by a slightly deeper embayment at the transition between the blade and the dorsal margin of the post-iliac process. The morphology of the blade in UMZC T.2013.3 (Fig. 4) conforms to the pattern described above, but detailed observations are hampered by slight disruption and the fact that the blade occurs in close proximity to disrupted skeletal elements, including a possible neural arch and some gastralia.

The post-iliac process has straight and parallel upper and lower margins, and terminates in a blunt squarish extremity. This pattern is conserved across all specimens. The process is orientated subhorizontally or slightly posterodorsally, extending nearly as far posteriorly as the rearmost extremity of the ischium.

Complete puboischiadic plates are observed in UMZC T.2013.3 and UMZC T.1350 (Figs 4, 6a, b), but sutures between the pubic and ischiadic portions are not discernible. Compaction implies that such plates are slightly flattened against the bedding plane. The ischia are elongate and subtrapezoidal, narrowing slightly in an anteroposterior direction. They are preserved in plan view in the holotype (Fig. 1), where their entire outline is clearly visible. Each ischium contacts its antimere along a straight ventral margin. We are unsure as to the precise course of this margin in side view, although there is some evidence (Fig. 4) that it may have been gently convex. The posterior margin of the bone is shaped approximately like a quarter of a circle (the posterior margins of both pubes would thus delimit a 'basin' in life), although this curvature would appear less accentuated in lateral view and has been altered by compaction (Figs 4, 6a, b). The posterior and dorsal margins of each ischium meet at a slightly obtuse angle (Fig. 1). The dorsal margin is shallowly convex throughout most of its length in the holotype and this convexity is somewhat discernible in other specimens as well. At its anteriormost extremity, the dorsal margin turns gently upward following a smoothly concave course, before merging into the posterior margin of the corpus of the ilium. This concave tract is seen in the holotype, but is scarcely visible in other specimens (Figs 4, 6a, b).

The pubis is much shorter than the ischium, its estimated length being less than half of the length of the latter bone. Although no isolated pubes are preserved along the bedding plane, those in articulation with the rest of the pelvic girdle possess a squarish or subtrapezoidal outline, with a distinct anteroventral corner and a smoothly convex anterodorsal edge connecting the anterior and dorsal margins of the bone (Figs 4, 6a, b). Its ventral margin may have been straight or gently concave in side view (Fig. 4).

No specimen shows a clearly defined acetabulum. A small depression at the junction between the anterior part of the corpus of the ilium and the dorsal part of the ischiadic plate in UMZC T.1350 (Fig. 6b) is tentatively interpreted as the poorly preserved anterodorsal section of the acetabulum.

3.7.4. Hind limb. As noted previously (Smithson 1994; Clack & Milner 2015), a distinctive feature of *Eldeceeon* is represented by its large and robust hind limbs. In NMS G.1990.7.1 (Fig. 2a), the length of the femur (measured as the greatest distance between the most proximal projection of its head to the most distal projection of its posterior, or fibular, condyle) is almost equal to the length of six trunk vertebrae. Similar proportions are estimated for the holotype (Fig. 1). The length of the femur exceeds that of the ischia (Fig. 1) and is comparable with the estimated length of the puboischiadic plates (Fig. 4). The best-preserved femora are observed in the holotype and in NMS G.1190.7.1 (Figs 1, 2a). In both specimens, their morphology conforms to the pattern of other anthracosauroids (e.g., Romer 1957; Panchen 1970; Holmes 1984, 1989; for easily accessible comparisons of femora among selected early tetrapods, see Ruta *et al.* 2001, fig. 12). The proximal and distal extremities of the bone are greatly expanded and of similar width, and are well delimited from the shaft. The shaft is relatively stocky and abbreviated. Both the anterior and the posterior margins are embayed. The distal condyles are robust, the fibular condyle being only slightly wider and projecting slightly more distally than the tibial condyle, and there is evidence of a short intercondylar space (albeit its outline is masked by compaction). In some of these features, the shape of the femur most closely resembles that of *Archeria crassidisca* (Holmes 1989; Ruta *et al.* 2001, fig. 12j) and, to a lesser degree, *Proterogyrinus scheelei* (Holmes 1984; Ruta *et al.* 2001, fig. 12k). In both these taxa, the tibial condyles are more robust than those of *Eldeceeon*, and comparable in size to the fibular condyles. A final note concerns the femora of NMS G.1990.7.1 (Fig. 2a), where the internal and fourth trochanter are discernible. In both femora, as preserved, the anterior margin of the proximal extremity protrudes slightly anteriorly forming a small, proximodistally elongate rectangular flange. We interpret this flange as the anteriormost projection of the internal trochanter (e.g., Panchen 1970, p. 37) in the extensor–flexor plane. The most proximal part of this flange terminates in a small and blunt process, representing the fourth trochanter (see Ruta *et al.* 2001, fig. 12).

All specimens show at least one complete or nearly complete tibia (Figs 1a, 2a, 4). In NMS G.1990.7.1, the proximal extremity of a contralateral element is also visible (Fig. 2a). The tibia of *Eldeceeon* is broadly similar to that of *Silvanerpeton* (Ruta & Clack 2006, figs 6a, 9a, b, 10c), but there are subtle differences between these two taxa. In *Eldeceeon*, the tibia has a more robust appearance with a comparatively broader and stouter proximal extremity than that of *Silvanerpeton*. In NMS G.1990.7.1, the complete outline of a fairly well-preserved tibia can be followed along the extensor/flexor plane of the bone. The bone shows wide proximal and distal extremities and a distinct short shaft. On the articulation surface of the proximal extremity of the tibia are two shallow condylar areas of slightly unequal extension, the anterior one appearing only marginally larger and shallower than the posterior one. The slightly raised area between the two condylar areas corresponds to the intercondylar ridge, an unremarkable low skeletal prominence in several anthracosauroids and other early tetrapods (e.g., Romer 1957; Panchen 1970; Holmes 1984, 1989), but well developed in *Eldeceeon*. Barring preservation artefacts, the projection of this ridge in the preserved view of the tibia is divided into a smaller anterior and a larger posterior eminence or tubercle. These eminences delimit a shallow space between them, presumably corresponding to an intercondylar groove in life. The distal extremity is vaguely subtrapezoidal

https://doi.org/10.1017/S1755691020000079 Published online by Cambridge University Press

and its anterior margin is slightly shorter than its posterior margin. As in the case of the proximal extremity, the margins end in distinct outer and inner angles. The distal margin has two distinct sections of approximately equal extension separated by a small triangular protrusion, for the articulation with the tibiale and intermedium bones. Their course is irregular, possibly as a result of preservation, but broadly concave along the intermedium contact and vaguely sinuous along the tibiale contact.

Both fibulae are preserved in the holotype (Fig. 1), in NMS G.1990.7.1 (Fig. 2a; only one element is visible in full), and in UMZC T.2013.3. Unlike *Silvanerpeton* (Ruta & Clack 2006, figs 6a, 9a, b, 10c), *Eldeceeon* possesses a comparatively more gracile fibula resembling that of anthracosauroids, such as *Archeria* and *Proterogyrinus* (e.g., Romer 1957; Panchen 1970; Holmes 1984, 1989). As preserved along the extensor/flexor plane, the fibula shows a very slightly expanded proximal extremity, with an irregularly convex proximal margin, a distinct anterior extension 'jutting out' towards the tibia, and an inconspicuous posterior extension. The shaft is slender and elongate and its anterior and posterior margins merge indistinctly into those of the proximal and distal extremities of the bone. The distal extremity forms a flat subtriangular blade with a strongly convex posterior margin and a gently sinuous anterior margin, which would be in contact with the intermedium (anteriorly) and fibulare (posteriorly).

Although heavily dislocated, the bones of the pes are preserved in close proximity in at least two specimens (Figs 1, 2a, 3c), permitting reasonable estimates of the proportions of the pes and individual digits (Smithson 1994). In other specimens, the pedal elements are too disrupted to permit accurate estimates of pedal proportions (Figs 4, 6a). We agree with Smithson's (1994) reconstruction of the pes as showing at least three proximal and five distal tarsal elements (e.g., Fig. 1), and we include a new reconstruction of the tarsus and pes in our new reconstruction of the skeleton (Fig. 7e). In NMS G.1990.7.1 (Figs 2a, 3c), the individual elements of a heavily disrupted pes are particularly well preserved. Scattered in close proximity to one another are five metatarsals and numerous phalanges. For a detailed account of the morphology of individual elements in this specimen, the reader is referred to the tracing of the pes (Fig. 3c). Tarsal and phalangeal elements appear to have been 'smeared' distally, not far from the tibia and fibula. Around each of these two bones, as well as between them, is a scatter of tarsals, three of which are distinctly larger than the rest, and are consistent with their interpretation as proximal tarsals. One of these, visible between the anterior corner of the proximal extremity of the tibia and the posterior margin of the shaft of the fibula, as preserved, is a conspicuous polygonal element, the shape of which is consistent with that of a pedal intermedium (e.g., Romer 1957; Holmes 1984, 1989; Smithson *et al*. 1994). Overlapped by the posterior corner of the distal extremity of the fibula, and arranged almost perpendicular to the latter, is a displaced metatarsal. Further to the right in the tracing of the pes, as figured, is a series of four metatarsals, arranged in approximately anatomical succession. Assuming that metatarsal I is the smallest of these four elements, it would correspond to the leftmost bone in the series. We note a curious gap in the series of four elements towards the rightmost of these. This gap appears to be well suited for the position of the metatarsal that lies transverse to the fibula, which would thus correspond to metatarsal IV. If our interpretation is correct, then the rightmost element in the series of four is metatarsal V. Metatarsals III and IV are approximately equal in length and comparable in robustness, and are slightly longer than metatarsals II and V. As for the phalanges, we count 18 elements scattered to the right of the metatarsals, as figured. This number would be consistent with an estimated phalangeal count of 2-3-4-5-4, but there is a difficulty. In the scatter of 18 bones, two or three are easily recognisable as distal phalanges (unguals), based on their small size and shape, being characteristically subtriangular, with deeply embayed lateral and mesial margins and a pointed distal tip. This, however, implies that at least another two or three unguals are undetected, unrecognised, or not preserved. Perhaps some poorly preserved bony fragments close to the tibia may represent unguals, but their interpretation is difficult. Assuming that our interpretation of the pes of NMS G.1990.7.1 is approximately correct, this raises the possibility that the phalangeal count of the pes may have been slightly higher.

3.8. Gastralia

The gastralia provide a broad cover for the ventral and, presumably, part of the lateral sides of the trunk and proximal tail region (Figs 1, 2a, 4). They appear similar in overall proportions to their homologues in *Silvanerpeton* (Ruta & Clack 2006, figs. 6, 7a, 9c), in being slender and elongate. Some show evidence of a central longitudinal ridge.

4. Phylogenetic analyses

The data matrix was not amenable to safe taxonomic reduction. Under maximum parsimony and with equally weighted characters, PAUP* produces nine trees at 1261 steps, with an ensemble consistency index (CI) of 0.2681 and an ensemble retention index (RI) of 0.5750. Their strict consensus (Fig. 8a) is fairly well resolved. With regard to the 'reptiliomorph' part of the phylogeny, the crownward succession of major groups includes: (1) a clade formed by *Eldeceeon* and *Silvanerpeton*; (2) chroniosuchians (represented by *Chroniosaurus dongusensis*); (3) a clade formed by *Solenodonsaurus* as sister taxon to the anthracosauroids *sensu* Smithson (1985) (i.e., eoherpetontids and embolomeres; Ruta & Clack 2006); (4) a clade of gephyrostegids [*Gephyrostegus bohemicus* + *Bruktererpeton fiebigi*]; (5) a clade of seymouriamorphs; (6) *Westlothiana*; (7) crown amniotes including monophyletic diadectomorphs as sister group to synapsids, and with largely unresolved diapsids (see also Klembara *et al*. 2020). Within the eoherpetontids–embolomeres clade, two main groups are retrieved: a group consisting of *Eoherpeton watsoni*, *Proterogyrinus pancheni*, *P. scheelei*, and [*Archeria crassidisca* + *Pholiderpeton scutigerum*] in a tetrachotomy; and a group consisting of *Anthracosaurus russelli* and *Palaeoherpeton decorum* as successive sister taxa, in that order, to a trichotomous group that includes *Eobaphetes kansensis*, *Pholiderpeton attheyi*, and [*Calligenethlon watsoni* + *Carbonoherpeton carrolli*]. Within seymouriamorphs, *Utegenia shpinari* is the sister taxon to a clade formed by seymouriids [*Seymouria baylorensis* + *S. sanjuanensis*] and karpinskiosaurids-discosauriscids, *Karpinskiosaurus secundus* joins [*Makowskia laticephala* + *Spinarerpeton brevicephalum*]; these three species join [(*Ariekanerpeton sigalovi* + *Discosauriscus austriacus*) + (*Leptoropha talonophora* + *Microphon exiguus*)]. Within diadectomorphs, *Limnoscelis paludis*, *Diasparactus zenos*, [*Diadectes absitus* + *D. sideropelicus*], and *Desmatodon hesperis* are successively more closely related, in that order, to [*Tseajaia campi* + *Orobates pabsti*]. Very few nodes are resolved in the 50 % majority-rule bootstrap and jackknife consensus topologies and support for resolved nodes is, with few exceptions, invariably weak (see Supplementary Material S4 and S5 for the bootstrap and jackknife consensus trees).

A single tree at 193.17075 steps is obtained when characters are reweighted by the maximum values of their consistency indexes from the initial unweighted analysis (CI = 0.4575; RI = 0.7717; Fig. 8b). In this tree, *Calligenethlon* and *Solenodonsaurus* form sister taxa and, together, they join the eoherpetontid–embolomere clade. Within embolomeres, *Proterogyrinus scheelei* is resolved as the sister taxon to

https://doi.org/10.1017/S1755691020000079 Published online by Cambridge University Press

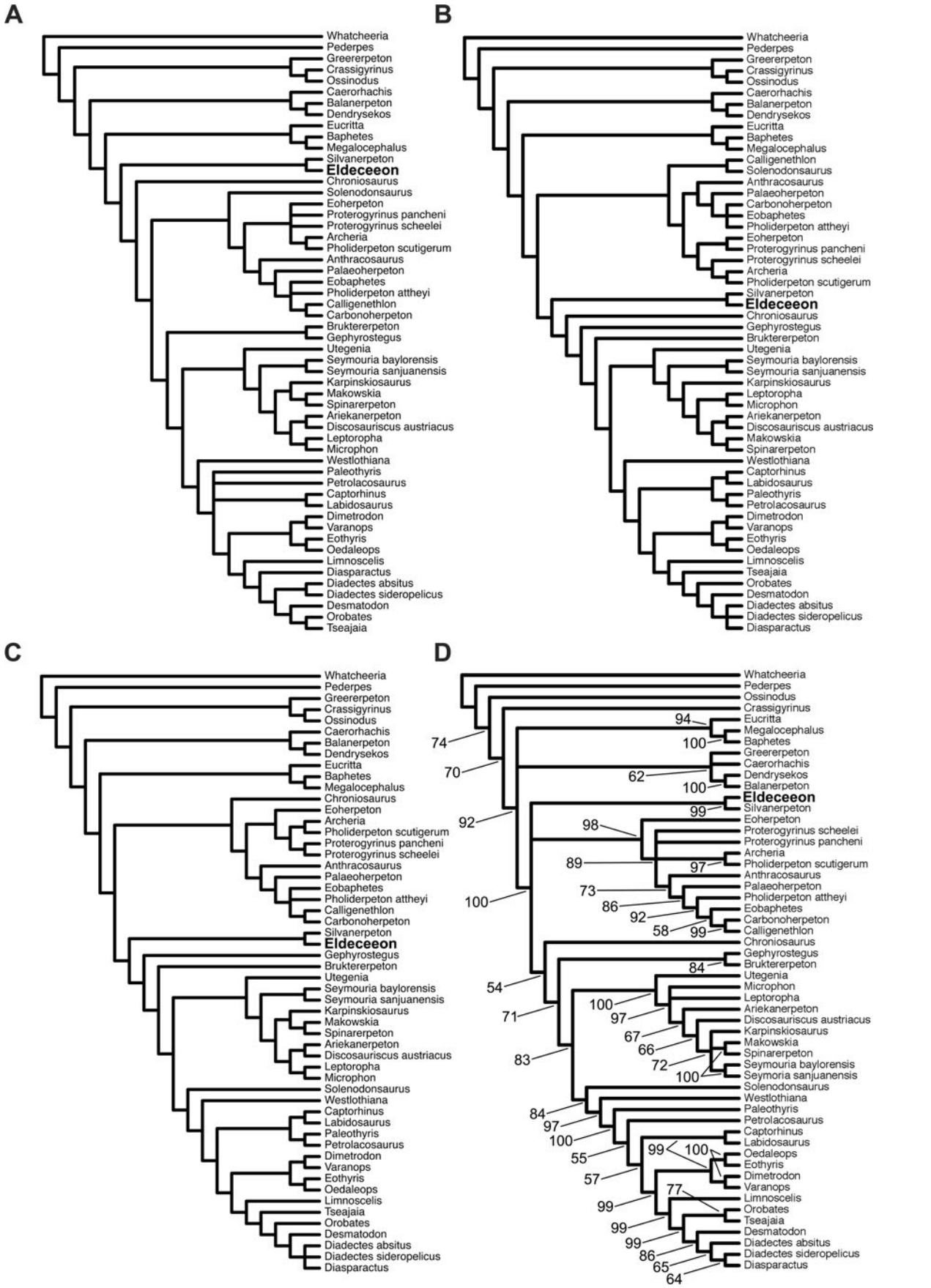

Figure 8 Interrelationships of *Eldeceeon rolfei*: four cladograms showing the position of this taxon in different phylogenetic experiments. (A) Strict consensus from analysis with unweighted characters. (B) Single tree from analysis with characters reweighted by the maximum values of their consistency indexes. (C) Single tree from analysis with implied weights, with constant of concavity $K = 6$. (D) Fifty percent majority-rule Bayesian consensus topology with clade credibility values appended to branches.

https://doi.org/10.1017/S1755691020000079 Published online by Cambridge University Press

[*Archeria*+ *Pholiderpeton scutigerum*], and this wider clade joins [*Eoherpeton* + *Proterogyrinus pancheni*]; in addition, *Carbonoherpeton*, *Eobaphetes*, and *Pholiderpeton attheyi* are collapsed in a trichotomy. *Silvanerpeton* and *Eldeceeon*, as sister taxa, branch from the amniote stem crownward of *Calligenethlon*–*Solenodonsaurus*–anthracosauroids. Crownward of [*Eldeceeon* + *Silvanerpeton*] is a paraphyletic array of taxa including, from less to more crownward, *Chroniosaurus*, *Gephyrostegus*, and *Bruktererpeton*. Within seymouriamorphs, *Karpinskiosaurus* is resolved as the sister taxon to discosauriscids. Within crown amniotes, diapsids are fully resolved and form the monophyletic sister group to a diadectomorph–synapsid clade. Finally, the branching sequence of diadectomorphs is largely overturned relative to that obtained in the unweighted analysis, with *Limnoscelis*, *Tseajaia*, *Orobates*, and *Desmatodon* forming a paraphyletic array relative to an unresolved clade encompassing *Diasparactus* and the two species of *Diadectes*.

In the four analyses with implied weights, the interrelationships of 'reptiliomorphs' are similar in some respects to those of the unweighted and weighted analyses and, therefore, only major differences are highlighted. The topologies of the single trees yielded by each of the analyses with $K = 9$ and 12 are identical. A single tree is obtained with $K = 6$, differing from the trees yielded by the analyses with $K = 9$ and 12 solely in the mutual arrangements of diapsids. For ease of discussion, we illustrate the single tree obtained with $K = 6$ (Fig. 8c). In this tree, *Solenodonsaurus* is assigned to a more crownward position than in the unweighted and weighted analyses, being the sister taxon to the clade formed by *Westlothiana* and crown amniotes. As in the reweighted analysis, gephyrostegids form a paraphyletic array, and the [*Eldeceeon* + *Silvanerpeton*] clade occurs immediately anti-crownward of this array. *Chroniosaurus* forms the sister taxon to anthracosauroids, the interrelationships of which agree with those from the unweighted analysis. The strict consensus of two trees yielded by the analysis with $K = 3$ (not illustrated) shows a few differences in the branching sequence of stem amniotes relative to the tree topologies discussed above. In particular, *Caerorhachis* emerges as the most plesiomorphic stem amniote (see also Ruta *et al.* 2001). *Chroniosaurus* forms the sister taxon to the [*Eldeceeon* + *Silvanerpeton*] clade, and this broader group is immediately crownward of anthracosauroids. Within the latter group, *Anthracosaurus* is sister taxon to all other anthracosauroids and *Solenodonsaurus* is deeply nested within the group. Further crownward, *Utegenia* branches from the amniote stem in an intermediate position between paraphyletic gephyrostegids and remaining seymouriamorphs.

The Bayesian analysis attained satisfactory convergence, with standard deviations of split frequencies much less than 0.1 and PSRF values approaching or equal to 1. The analysis produces good to excellent support for several nodes, as shown by their credibility values (reported below in brackets; Fig. 8d). The branching sequence of most major groups largely agrees with those yielded by the parsimony analyses. Strong support is assigned to the [*Eldeceeon* + *Silvanerpeton*] clade (99), anthracosauroids (98), gephyrostegids (84), the branch subtending gephyrostegids and immediately more crownward groups (71), seymouriamorphs (100), the branch subtending seymouriamorphs and immediately more crownward groups (83), the branch subtending *Solenodonsaurus* and immediately more crownward groups (84), the branch subtending *Westlothiana* and immediately more crownward groups (97), crown amniotes inclusive of diadectomorphs (100), and the branches subtending synapsids, diadectomorphs, and both of these groups as sister clades (99). Additional branches in each major group also receive high credibility values (Fig. 8d). The position of [*Eldeceeon* + *Silvanerpeton*] in relation to anthracosauroids and more derived groups is unresolved in the Bayesian tree. In addition, no support emerges for diapsids. *Chroniosaurus* forms the sister taxon to gephyrostegids and all more crownward groups, albeit with weak support (54).

5. Discussion

5.1. Skeletal construction and lifestyle of *Eldeceeon*

The unique combination of postcranial features of *Eldeceeon* – especially the remarkable size difference between its anterior and posterior limbs and the proportions and distribution of its trunk ribs (Fig. 7e) – invites a brief consideration of its locomotory adaptations. Biomechanical studies of fossil amniotes are aided by close comparisons with modern taxa (e.g., Bates *et al.* 2015). Although *Eldeceeon* is removed from any suitable analogue among extant or extinct crown amniotes, and its mode of preservation make it impossible to conduct three-dimensional modelling of locomotory performance, we think it useful to comment on the possible functional implications of its skeletal construction.

The most vexing aspect of the *Eldeceeon* postcranium is the configuration of its rib cage (Smithson 1994; Fig. 7e), with long and curved ribs confined to the anterior half of its trunk. We hypothesise that the space between the most posterior trunk ribs and the pelvis was occupied by an unusually large *puboischiofemoralis internus 2* (PIFI2). In modern alligators, PIFI2 originates on the centra of the lumbar vertebrae (most posterior presacrals) as well as on the ventral surfaces of their transverse processes, and inserts on the anterodorsal aspect of the proximal femur (Reilly *et al.* 2005). In *Eldeceeon*, the origin of the PIFI2 fibres may have extended further forward along the posterior half of the vertebral column than in a modern alligator, such that a considerably greater number of presacrals may have provided sites for muscle attachment. Two consequences of this arrangement are that (1) several PIFI2 fibres were proportionally (i.e., accounting for scale) longer and (2) the mass and volume of PIFI2 were proportionally greater in *Eldeceeon* than in an alligator. If the PIFI2 volume increases (in relation to a hypothetical ancestral condition in which the PIFI2 is restricted to the rearmost part of the trunk), then the physiological cross-sectional area of the muscle (the ratio between muscle volume and fibre length) augments, resulting in greater force production during contraction. As for the attachment area of the PIFI2 on the *Eldeceeon* femur, this was most likely represented by its robust internal trochanter.

The morpho-functional system we have described corresponds to a class 3 lever, with the fulcrum situated at the articulation between the femur and the pelvis, the load represented by the weight of the hind limb, and the effort (the force exerted by the contracting PIFI2) located at the insertion of the PIFI2 on the femur (between the fulcrum and the load). While not mechanically advantageous, this system ensures considerable excursion for the hind limb, allowing the femur to swing forward and upward, perhaps in rapid bursts, during the forward phase of the stride cycle. However, even assuming our hypothesis about the PIFI2 is correct, it is unclear why *Eldeceeon* developed such powerful and large hind limbs in the first instance, particularly as far as the dimensions of its pes are concerned. As in the original reconstruction (Smithson 1994), and as confirmed by the present study (Fig. 7e), the pes proportions imply that, when the hind limb was fully extended forward, the distal extremity of the longest digit would be approximately aligned vertically with the most anterior trunk ribs. We propose that such unusual pes proportions enabled *Eldeceeon* to run fast through an increase in the stride length and a concomitant reduction in the stride frequency (for a detailed discussion, see Aerts *et al.* 2000). These requirements necessitate increase in muscle force

https://doi.org/10.1017/S1755691020000079 Published online by Cambridge University Press

(see discussion of PIFI2 above), but would also result in fewer muscle contractions. A possible biomechanical trade-off may have been achieved through the evolution of a large pes with long toes, which probably facilitated propulsion forward during the last phase of a stride cycle, when the hind limb was fully extended backward. Repositioning the foot anteriorly would have required strong muscles to pull the femur upward, causing it to rotate simultaneously inward and forward, and to lift the toes off the ground. Consistent with the morpho-functional requirements associated with high speed and augmented stride length is the apparent absence of ossified carpal elements in *Eldeceeon*, which may represent a weight-reducing adaptation.

5.2. *Eldeceeon* and the amniote stem group

Despite its general resemblance to other anthracosauroid 'reptiliomorphs', *Eldeceeon rolfei* is sufficiently distinct from all described species in this group. Comparisons between *Eldeceeon* and *Silvanerpeton miripedes* were summarised in previous publications (Clack 1994; Smithson 1994; Clack & Milner 2015) and have been highlighted in the descriptive sections of the present paper. Therefore, they will not be repeated here and only a summary of key points is provided below.

The affinities of *Eldeceeon* with anthracosauroid 'reptiliomorphs' (though not necessarily its assignment to this group) are suggested by the general configuration of the skull (note: other tetrapod groups may show combinations of some of the features listed below), including: (1) a tabular 'horn' (more specifically, the preserved superficial or 'dermal' component of the horn; in *Silvanerpeton*, there is some evidence of the subdivision of the horn into a superficial and a deep component); (2) slightly convex lateral margins of the skull table formed by the bones of the lateral temporal series (in *Silvanerpeton*, such margins are approximately straight in dorsal aspect); (3) 'dominance' of the supratemporal, which is at least marginally larger than the intertemporal and the tabular (in *Silvanerpeton*, the intertemporal is the largest of the three bones in the temporal series); (4) a deep suspensorium with a nearly straight and oblique posterior margin in lateral aspect, with a small notch in its dorsalmost portion (in *Silvanerpeton*, the margin of the suspensorium is shallowly concave and there is no evidence of a deep dorsal embayment); (5) a hinge-like contact between the cheek and the skull table (the situation in *Silvanerpeton* is less clear); (6) presumably moveable basicranial articulation (also in *Silvanerpeton*); (7) 'closed' (or nearly closed) palate (also in *Silvanerpeton*); (8) broad pterygoids with poor delimitation among the palatal ramus, the corpus, and the quadrate ramus (also in *Silvanerpeton*); (9) presumably fang-less vomers (in *Silvanerpeton*, two small teeth and irregular denticle rows are present; the absence of dentition in *Eldeceeon* is not entirely certain); (10) deepening of the lower jaw in its posterior half, involving various degrees of dorsoventral expansion of the squama of the angular (in *Silvanerpeton*, there is only weak evidence of a posterior deepening of the jaw ramus). Some characters from the postcranium also indicate anthracosauroid affinities for *Eldeceeon*, including: (11) notochordal gastrocentrous vertebrae (also in *Silvanerpeton*); (12) markedly curved ribs, at least along the thoracic part of the trunk (also in *Silvanerpeton* in which, however, elongate ribs occupy the entire trunk length); (13) various degrees of elongation of the parasternal process of the interclavicle (in *Silvanerpeton*, the interclavicle is kite-shaped with an elongate triangular parasternal process; in *Eldeceeon*, the parasternal process is long and narrow); and (14) bifurcated ilium consisting of a subquadrangular dorsal blade and a rod-like post-iliac process (also in *Silvanerpeton*).

The characters listed above rule out the affinities of *Eldeceeon* with other major groups of 'reptiliomorphs', such as seymouriamorphs and gephyrostegids (Ruta & Clack 2006; Klembara *et al.* 2014). *Eldeceeon* bears only a vague resemblance to discosauriscid seymouriamorphs (e.g., Klembara 1997; Klembara & Ruta 2004a, b, 2005a, b), especially in its deep skull, enlarged orbits, relatively foreshortened snout region, and proportions of the anterior part of the lower jaw ramus (Fig. 7a–d). However, details of individual bones of the skull and postcranium of seymouriamorphs in general, and discosauriscids in particular (e.g., outline and proportions of the skull table, shape of the ilium), bar *Eldeceeon* from seymouriamorphs as a whole. Similar reasoning applies to gephyrostegids (see Carroll 1970; Klembara *et al.* 2014). Although anthracosauroid affinities have been proposed for this group (summary in Klembara *et al.* 2014), their putative shared characters are now generally considered to be generalised and possibly plesiomorphic, and thus cannot be used to link *Eldeceeon* specifically to gephyrostegids. No cranial or postcranial traits regarded as being unique to gephyrostegids occur in *Eldeceeon*. Finally, one of the three cranial characters that gephyrostegids share with seymouriamorphs (Klembara *et al.* 2014) – namely, a rectangular outline of the transverse process of the pterygoid – is also documented in *Eldeceeon*. Due to preservation, however, the other two characters (radiating rows of closely packed denticles on the palate; a wedge-like triangular process on the parasphenoid) cannot be observed.

6. Conclusions

The present contribution both augments our understanding of the comparative skeletal anatomy of East Kirkton tetrapods and adds to our knowledge of character distribution among stem amniotes. The anatomy of the axial and appendicular skeleton of *Eldeceeon* contrasts with its fairly unspecialised craniodental morphology, adding to our knowledge of morpho-functional adaptations exhibited by early tetrapods during the Mississippian, including novel feeding and locomotory strategies and a diverse range of body proportions (Anderson *et al.* 2015; Clack *et al.* 2016, 2019; Clack 2017; Smithson & Clack 2018; Ruta *et al.* 2019). The large hind feet and elongate toes of *Eldeceeon* presumably enabled this animal to attain high locomotory speed though increasing stride length. However, its robust hind limbs presumably required large and powerful muscle contractions during the forward phase of the locomotory cycle. To compensate for the poor mechanical advantage afforded by this type of lever system, stride frequency (and, thus, the number of muscle contractions) was presumably reduced. We posit that the PIFI2 (or an analogue of this muscle), chiefly responsible for the hind limb forward rotation, was particularly enlarged in *Eldeceeon*, and its anteriormost extremity probably extended along the posterior half of the vertebral column, which may account for the distribution of long, curved ribs in the anterior half of the trunk. Despite their conflicting placements relative to other 'reptiliomorphs' in different treatments of our data matrix, *Eldeceeon* and *Silvanerpeton* provide unique insights into the polarity of cranial and postcranial traits near the evolutionary roots of amniote diversity.

7. Dedication

On 26 March 2020, our good friend and valued colleague Jenny Clack died after living with cancer for five years. During the mid-1980s, Jenny became a founding member of the East Kirkton Project. She attended its first meeting at the East Kirkton Quarry in 1985 as well as a major international conference on early terrestrial biota held in Edinburgh in 1992, where research on East Kirkton featured conspicuously (Rolfe *et al.* 1994; Clack 2017). Jenny named and described three tetrapods from the site: *Silvanerpeton miripedes*, *Eucritta melanolimnetes*, and *Kirktonecta milnerae* (Clack 1994, 1998, 2011). The present

https://doi.org/10.1017/S1755691020000079 Published online by Cambridge University Press

contribution is the last paper that she saw all the way through to submission and first round of revision. It is also the work that brought her back to East Kirkton, and further papers initiated by her are now in the pipeline. Despite her illness, Jenny continued working with unswerving dedication, enthusiasm, and passion until her last few days. In 1977, access to the type specimen of the anthracosaur *Pholiderpeton scutigerum*, the subject of her PhD dissertation (Clack 1983, 1987), marked the beginning of Jenny's scientific career. We are saddened that Jenny cannot see the final instalment of our joint efforts on *Eldeceeon*. However, we think she would be delighted to see this additional contribution to her pet tetrapod group.

8. Acknowledgements

We are indebted to Mathew Lowe and Jason Head (UMZC) and to Stig Walsh and Nicholas Fraser (National Museums Scotland, Edinburgh) for access to specimens in their care. We thank Lorie J. Barber (formerly, Bristol Museum and Art Gallery) for carrying out preparation of specimen UMZC T.1350. We are grateful to Stig Walsh (Editor, *EESTRSE*) and Susie Cox (Editorial Office, *EESTRSE*) for their assistance through all stages of manuscript production. Finally, we are indebted to Jozef Klembara (Comenius University, Bratislava) and Angela Milner (Natural History Museum, London) for their constructive comments and encouraging feedback.

9. Supplementary material

Supplementary material is available online at https://doi.org/10.1017/S1755691020000079.

10. References

Aerts, P., Van Damme, B., Vanhooydonck, B., Zaaf, A. & Herrel, A. 2000. Lizard locomotion: how morphology meets ecology. *Netherlands Journal of Zoology* **50**, 261–77.

Anderson, J. S., Smithson, T., Mansky, C. F., Meyer, T. & Clack, J. A. 2015. A diverse tetrapod fauna at the base of 'Romer's Gap'. *PLoS ONE* **10**, 1–27.

Arbez, T., Sidor, C. A. & Steyer, J.-S. 2019. *Laosuchus naga* gen. et sp. nov., a new chroniosuchian from South-East Asia (Laos) with internal structures revealed by micro-CT scan and discussion of its palaeobiology. *Journal of Systematic Palaeontology* **17**, 945–62.

Bates, K., Maidment, S. C. R., Schachner, E. R. & Barrett, P. M. 2015. Comments and corrections on 3D modelling studies of locomotor muscle moment arms in archosaurs. *PeerJ* **3**, e1272.

Bystrow, A. P. & Efremov, I. A. 1940. *Benthosuchus sushkini* Efr. – a labyrinthodont from the Eotriassic of Sharzhenga river. *Trudy Paleontologičeskogo Instituta Akademii Nauk SSSR* **10**, 1–152. [in Russian.]

Carroll, R. L. 1970. The ancestry of reptiles. *Philosophical Transactions of the Royal Society of London, Series B* **257**, 267–308.

Carroll, R. L., Bossy, K. A., Milner, A. C., Andrews, S. M. & Wellstead, C. F. 1998. *Handbook of paleoherpetology, part 1: Lepospondyli*. München: Verlag Dr. Friedrich Pfeil. 216 pp.

Clack, J. A. 1983. The stapes of the Coal Measures embolomere *Pholiderpeton scutigerum* Huxley and otic evolution in early tetrapods. *Zoological Journal of the Linnean Society* **79**, 121–48.

Clack, J. A. 1987. *Pholiderpeton scutigerum* Huxley, an amphibian from the Yorkshire Coal Measures. *Philosophical Transactions of the Royal Society of London, Series B* **318**, 1–107.

Clack, J. A. 1994. *Silvanerpeton miripedes*, a new anthracosauroid from the Viséan of East Kirkton, West Lothian, Scotland. *Transactions of the Royal Society of Edinburgh: Earth Sciences* **84**, 369–76.

Clack, J. A. 1998. A new Early Carboniferous tetrapod with a *mélange* of crown-group characters. *Nature* **394**, 66–69.

Clack, J. A. 2001. *Eucritta melanolimnetes* from the Early Carboniferous of Scotland, a stem tetrapod showing a mosaic of characteristics. *Transactions of the Royal Society of Edinburgh: Earth Sciences* **92**, 75–95.

Clack, J. A. 2011. A new microsaur from the early Carboniferous (Viséan) of East Kirkton, Scotland, showing soft tissue evidence. *Special Papers in Palaeontology* **86**, 1–11.

Clack, J. A. 2012. *Gaining ground: the origin and evolution of tetrapods*. 2nd edn. Bloomington, Indiana: Indiana University Press. 523 pp.

Clack, J. A. 2017. The East Kirkton Lagerstätte: a window onto Early Carboniferous land ecosystems. *In* Fraser, N. C. & Sues, H. D. (eds) *Terrestrial conservation lagerstätten: windows into the evolution of life on land*, 39–64. Edinburgh: Dunedin Academic Press.

Clack, J. A., Bennett, C. E., Carpenter, D. K., Davies, S. J., Fraser, N. C., Kearsey, T. I., Marshall, J. E. A., Millward, D., Otoo, B. K. A., Reeves, E. J., Ross, A. J., Ruta, M., Smithson, K. Z., Smithson, T. R. & Walsh, S. A. 2016. Phylogenetic and environmental context of a Tournaisian tetrapod fauna. *Nature Ecology and Evolution* **1**, 1–11.

Clack, J. A., Ruta, M., Milner, A. R., Marshall, J. E. A., Smithson, T. R. & Smithson, K. Z. 2019. *Acherontiscus caledoniae*: the earliest heterodont and durophagous tetrapod. *Royal Society Open Science* **6**, 1–10.

Clack, J. A. & Finney, S. M. 2005. *Pederpes finneyae*, an articulated tetrapod from the Tournaisian of Western Scotland. *Journal of Systematic Palaeontology* **2**, 311–46.

Clack, J. A. & Klembara, J. 2009. An articulated specimen of *Chroniosaurus dongusensis* and the morphology and relationships of the chroniosuchids. *Special Papers in Palaeontology* **81**, 15–42.

Clack, J. A. & Milner, A. R. 2015. *Handbook of paleoherpetology, part 3A1: basal Tetrapoda*. München: Verlag Dr. Friedrich Pfeil. 93 pp.

Danto, M., Witzmann, F. & Müller, J. 2012. Redescription and phylogenetic relationships of *Solenodonsaurus janenschi* Broili, 1924, from the Late Carboniferous of Nýřany, Czech Republic. *Fossil Record* **15**, 45–59.

Farris, J. S., Albert, V. A., Källersjö, M., Lipscomb, D. & Kluge, A. G. 1996. Parsimony jackknifing outperforms neighbor-joining. *Cladistics* **12**, 99–124.

Felsenstein, J. 1985. Confidence limits on phylogenies: An approach using the bootstrap. *Evolution* **39**, 783–91.

Ford, D. P. & Benson, R. B. J. 2019. A redescription of *Orovenator mayorum* (Sauropsida, Diapsida) using high resolution µCT, and the consequences for early amniote phylogeny. *Papers in Palaeontology* **5**, 197–239.

Fraser, N. C., Smithson, T. R. & Clack, J. A. (eds) 2018. *A legacy in fossils: a tribute to Stan Wood. Earth and Environmental Science Transactions of the Royal Society of Edinburgh*, vol. **108**. Cambridge: Cambridge University Press. 117 pp.

Gelman, A. & Rubin, D. B. 1992. Inference from iterative simulation using multiple sequences. *Statistical Science* **7**, 457–72.

Goloboff, P. 1993. Estimating character weighting during tree search. *Cladistics* **9**, 83–91.

Goloboff, P. A., Torres, A. & Arias, J. S. 2018. Weighted parsimony outperforms other methods of phylogenetic inference under models appropriate for morphology. *Cladistics* **34**, 407–37.

Goodrich, E. S. 1916. On the classification of the Reptilia. *Proceedings of the Royal Society of London. Series B* **89**, 261–76.

Haeckel, E. 1866. *Generelle Morphologie der Organismen: allgemeine Grundzüge der organischen Formen-Wissenschaft, mechanisch begründet durch die von Charles Darwin reformirte Descendenz-Theorie*. Berlin: Verlag von Georg Reimer. 574 pp.

Holmes, R. B. 1984. The Carboniferous amphibian *Proterogyrinus scheelei* Romer, and the early evolution of tetrapods. *Philosophical Transactions of the Royal Society of London, Series B* **306**, 431–527.

Holmes, R. B. 1989. The skull and axial skeleton of the Lower Permian anthracosauroid amphibian *Archeria crassidisca* Cope. *Palaeontographica Abteilung A* **207**, 161–206.

Jaekel, O. 1909. Über die Klassen der Tetrapoden. *Zoologischer Anzeiger* **34**, 193–212.

Jarvik, E. 1996. The Devonian tetrapod *Ichthyostega*. *Fossils & Strata* **40**, 1–206.

Kathe, W. 1999. Comparative morphology and functional interpretation of the sutures in the dermal skull roof of temnospondyl amphibians. *Zoological Journal of the Linnean Society* **126**, 1–39.

Klembara, J. 1997. The cranial anatomy of *Discosauriscus* Kuhn, a seymouriamorph tetrapod from the Lower Permian of the Boskovice Furrow (Czech Republic). *Philosophical Transactions of the Royal Society of London B* **352**, 257–302.

Klembara, J., Clack, J. A., Milner, A. R. & Ruta, M. 2014. Cranial anatomy, ontogeny, and relationships of the Late Carboniferous tetrapod *Gephyrostegus bohemicus* Jaekel, 1902. *Journal of Vertebrate Paleontology* **34**, 774–92.

Klembara, J., Hain, M., Ruta, M., Berman, D. S., Pierce, S. E. & Henrici, A. C. 2020. Inner ear morphology of diadectomorphs and seymouriamorphs (Tetrapoda) uncovered by high-resolution x-ray microcomputed tomography, and the origin of the amniote crown-group. *Palaeontology* **63**, 131–54.

Klembara, J. & Bartík, I. 2000. The postcranial skeleton of *Discosauriscus* Kuhn, a seymouriamorph tetrapod from the Lower Permian of the Boskovice Furrow (Czech Republic). *Transactions of the Royal Society of Edinburgh: Earth Sciences* **90**, 287–316.

Klembara, J. & Ruta, M. 2004a. The seymouriamorph tetrapod *Utegenia shpinari* from the ?Upper Carboniferous–Lower Permian of Kazakhstan. Part I: cranial anatomy and ontogeny. *Transactions of the Royal Society of Edinburgh: Earth Sciences* **94**, 45–74.

Klembara, J. & Ruta, M. 2004b. The seymouriamorph tetrapod *Utegenia shpinari* from the ?Upper Carboniferous–Lower Permian of Kazakhstan. Part I: postcranial anatomy and relationships. *Transactions of the Royal Society of Edinburgh: Earth Sciences* **94**, 75–93.

Klembara, J. & Ruta, M. 2005a. The seymouriamorph tetrapod *Ariekanerpeton sigalovi* from the Lower Permian of Tadzhikistan. Part I: cranial anatomy and ontogeny. *Transactions of the Royal Society of Edinburgh: Earth Sciences* **96**, 43–70.

Klembara, J. & Ruta, M. 2005b. The seymouriamorph tetrapod *Ariekanerpeton Sigalovi* from the Lower Permian of Tadzhikistan. Part II: postcranial anatomy and relationships. *Transactions of the Royal Society of Edinburgh: Earth Sciences* **96**, 71–93.

Laurin, M. 2001. L'utilisation de la taxonomie phylogénétique en paléontologie: Avatages et inconvénients. *Biosystema* **19**, 197–211.

Laurin, M. & Reisz, R. R. 1999. A new study of *Solenodonsaurus janenschi*, and a reconsideration of amniote origins and stegocephalian evolution. *Canadian Journal of Earth Sciences* **36**, 1239–55.

Lloyd, G. T. 2016. Estimating morphological diversity and tempo with discrete character-taxon matrices: implementation, challenges, progress, and future directions. *Biological Journal of the Linnean Society* **118**, 131–51.

Marjanović, D. & Laurin, M. 2019. Phylogeny of Paleozoic limbed vertebrates reassessed through revision and expansion of the largest published relevant data matrix. *PeerJ* **6**, 1–191.

Milner, A. C. 1994. The aïstopod amphibian from the Viséan of East Kirkton, West Lothian, Scotland. *Transactions of the Royal Society of Edinburgh: Earth Sciences* **84**, 363–68.

Milner, A. R. & Sequeira, S. E. K. 1994. The temnospondyl amphibians from the Viséan of East Kirkton, West Lothian. *Scotland. Transactions of the Royal Society of Edinburgh: Earth Sciences* **84**, 331–61.

Panchen, A. L. 1970. *Handbuch der Paläoherpetologie, Teil 5A: Anthracosauria*. Stuttgart: Gustav Fischer Verlag. 84 pp.

Panchen, A. L. & Smithson, T. R. 1988. The relationships of early tetrapods. *In* Benton, M. J. (ed.) *The phylogeny and classification of the tetrapods 1, amphibians, reptiles, birds*, 1–32. Oxford: Clarendon Press.

Pardo, J. D., Szostakiwskyj, M., Ahlberg, P. E. & Anderson, J. S. 2017. Hidden morphological diversity among early tetrapods. *Nature* **546**, 642–45.

Reilly, S. M., Willey, J. S., Biknevicius, A. R. & Blob, R. W. 2005. Hindlimb function in the alligator: integrating movements, motor patterns, ground reaction forces and bone strain of terrestrial locomotion. *Journal of Experimental Biology* **208**, 993–1009.

Rolfe, W. D. I., Clarkson, E. N. K & Panchen, A. L. (eds) 1994. *Volcanism and early terrestrial biota. Transactions of the Royal Society of Edinburgh: Earth Sciences*, vol. **84**, Edinburgh: The Royal Society of Edinburgh. 467 pp.

Romer, A. S. 1957. The appendicular skeleton of the Permian embolomerous amphibian *Archeria*. *Contributions from the Museum of Palaeontology, University of Michigan* **13**, 103–59.

Ronquist, F. & Huelsenbeck, J. P. 2003. MRBAYES 3: Bayesian phylogenetic inference under mixed models. *Bioinformatics* **19**, 1572–74.

Ruta, M., Milner, A. R. & Coates, M. I. 2001. The tetrapod *Caerorhachis bairdi* Homes and Carroll from the Lower Carboniferous of Scotland. *Transactions of the Royal Society of Edinburgh: Earth Sciences* **92**, 229–61.

Ruta, M., Coates, M. I. & Quicke, D. L. J. 2003. Early tetrapod relationships revisited. *Biological Reviews* **78**, 251–345.

Ruta, M., Krieger, J., Angielczyk, K. A. & Wills, M. A. 2019. The evolution of the tetrapod humerus: Morphometrics, disparity, and evolutionary rates. *Earth and Environmental Science Transactions of the Royal Society of Edinburgh* **109**, 351–69.

Ruta, M. & Bolt, J. R. 2006. A reassessment of the temnospondyl amphibian *Perryella olsoni* from the Lower Permian of Oklahoma. *Transactions of the Royal Society of Edinburgh: Earth Sciences* **97**, 113–65.

Ruta, M. & Clack, J. A. 2006. A review of *Silvanerpeton miripedes*, a stem amniote from the Lower Carboniferous of East Kirkton, West Lothian, Scotland. *Transactions of the Royal Society of Edinburgh: Earth Sciences* **97**, 31–63.

Ruta, M. & Coates, M. I. 2007. Dates, nodes and character conflict: Addressing the lissamphibian origin problem. *Journal of Systematic Palaeontology* **5**, 69–122.

Säve-Söderbergh, G. 1934. Some points of view concerning the evolution of the vertebrates and the classification of this group. *Arkiv för Zoologi* **26A**, 1–20.

Schoch, R. R. 2013. The evolution of major temnospondyl clades: an inclusive phylogenetic analysis. *Journal of Systematic Palaeontology* **11**, 673–705.

Schoch, R. R., Voigt, S. & Buchwitz, M. 2010. A chroniosuchid from the Triassic of Kyrgyzstan and analysis of chroniosuchian relationships. *Zoological Journal of the Linnean Society* **160**, 515–30.

Schoch, R. R. & Milner, A. R. 2014. *Handbook of paleoherpetology, part 3A2: Temnospondyli I*. München: Verlag Dr. Friedrich Pfeil. 150 pp.

Smithson, T. R. 1985. The morphology and relationships of the Carboniferous amphibian *Eoherpeton watsoni* Panchen. *Zoological Journal of the Linnean Society* **85**, 317–410.

Smithson, T. R. 1989. The earliest known reptile. *Nature* **342**, 676–78.

Smithson, T. R. 1994. *Eldeceeon rolfei*, a new reptiliomorph from the Viséan of East Kirkton, West Lothian, Scotland. *Transactions of the Royal Society of Edinburgh: Earth Sciences* **84**, 377–82.

Smithson, T. R., Carroll, R. L., Panchen, A. L. & Andrews, S. M. 1994. *Westlothiana lizziae* from the Viséan of East Kirkton, West Lothian, Scotland, and the amniote stem. *Transactions of the Royal Society of Edinburgh: Earth Sciences* **84**, 383–412.

Smithson, T. R. & Clack, J. A. 2018. A new tetrapod from Romer's Gap reveals an early adaptation for walking. *Earth and Environmental Science Transactions of the Royal Society of Edinburgh* **108**, 89–97.

Smithson, T. R. & Rolfe, W. D. I. 1990. *Westlothiana* gen. nov.: naming the earliest known reptile. *Scottish Journal of Geology* **26**, 137–38.

Sues, H.-D. 2019. Authorship and date of publication of the name Tetrapoda. *Journal of Vertebrate Paleontology* **39**, e1564758.

Swofford, D. L. 1998. *PAUP* Phylogenetic analysis using parsimony* (**and other methods*). *Version* 4. Sunderland, Massachusetts: Sinauer Associates.

White, T. E. 1939. Osteology of *Seymouria baylorensis* Broili. *Bulletin of the Museum of Comparative Zoology* **85**, 325–409.

Wilkinson, M. 1996. Majority-rule reduced consensus trees and their use in bootstrapping. *Molecular Biology and Evolution* **13**, 437–44.

Witzmann, F. & Schoch, R. R. 2018. Skull and postcranium of the bystrowianid *Bystrowiella schumanni* from the Middle Triassic of Germany, and the position of chroniosuchians within Tetrapoda. *Journal of Systematic Palaeontology* **16**, 711–39.

MS received 7 January 2020. Accepted for publication 11 June 2020. First published online 10 August 2020